THE JOURNAL OF PHYSICAL CHEMISTRY C
A JOURNAL OF THE AMERICAN CHEMICAL SOCIETY

pubs.acs.org/JPCC

Review

Solid-State Nuclear Magnetic Resonance Studies of Lithium and Sodium Metal Batteries

Published as part of The Journal of Physical Chemistry C special issue "Spectroscopic Techniques for Renewable Energy".

Bizhu Zheng, Xiangsi Liu,* and Yuxuan Xiang*

Cite This: J. Phys. Chem. C 2024, 128, 18659−18677

Read Online

ACCESS | Metrics & More | Article Recommendations

ABSTRACT: Lithium/sodium metal batteries have become a pivotal focus in the field of rechargeable batteries due to their potential to offer the highest specific capacity and lowest operating voltage. However, this high energy density brings significant instability between the lithium/sodium metal anode and the electrolyte. This instability can lead to uneven lithium/sodium deposits, known as dendrites or mossy type deposits, and uncontrolled formation of solid electrolyte interphases (SEIs), which further impede the ionic transport of working ions at the interface. Understanding the origins of morphological evolution, side reactions, and ion transport at the alkali metal/electrolyte interface is crucial for improving the cycle life of lithium/sodium metal batteries. Solid-state NMR, with its ability to provide detailed information about the chemistry, morphology, and ionic dynamics, is becoming an indispensable technique for studying metal anodes. In this review, we first introduce the basics of NMR in studying metal anodes and then select specific examples to illustrate how various NMR methods, including multinuclear magic angle spinning (MAS) NMR, electrochemical *in situ* NMR, and NMR dynamics methods, provide unique insights into the chemical composition of SEIs, deposit morphological evolution, and ionic dynamics at the lithium metal/electrolyte interface.

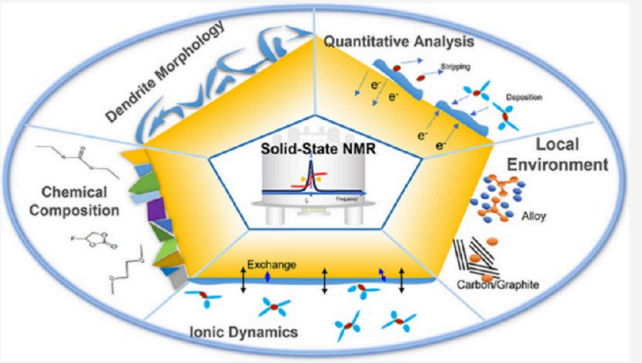

1. INTRODUCTION

Metal anodes, including lithium, sodium, and zinc, are considered promising alternatives for various rechargeable battery chemistries due to their high specific capacities. Lithium metal anodes, in particular, offer the highest specific capacity (3860 mAh/g) and the lowest electrochemical potential (−3.04 V vs SHE),[1] making them capable of delivering superior energy density when used as anode materials. However, their practical application is hindered by several critical challenges. The extremely low working voltage often exceeds the stability limits of current electrolyte systems, leading to irreversible side reactions at the metal/electrolyte interface. Moreover, in the absence of a suitable host material during cycling, lithium tends to deposit in a mossy or dendritic morphology with a high surface area, exacerbating side reactions. This irregular deposition contributes to the formation of inactive lithium during subsequent discharge cycles, resulting in significant lithium inventory loss and severely limiting the practical application of lithium metal anodes.[2−5]

A thorough understanding of the failure mechanisms in lithium metal batteries necessitates detailed insights into interfacial reactions, morphological evolution, and ionic transport at the lithium metal−electrolyte interface, challenges that are not easily addressed by current characterization techniques. Solid-state nuclear magnetic resonance (NMR) spectroscopy, with its diverse methodological approaches, is uniquely positioned to overcome these challenges.[6,7] NMR stands out as the only technique capable of providing simultaneous chemical, morphological, and ionic transport information. Magic angle spinning (MAS) NMR can mitigate various nuclear interactions, yielding high-resolution spectra that precisely analyze chemical products, regardless of crystallinity. The bulk magnetic effects of metals induce chemical shifts influenced by their orientation in the magnetic field, providing crucial insights into the morphology of the

Received: August 29, 2024
Revised: October 12, 2024
Accepted: October 15, 2024
Published: October 25, 2024

https://doi.org/10.1021/acs.jpcc.4c05822
J. Phys. Chem. C 2024, 128, 18659−18677

lithium metal. Dynamic NMR methods, such as relaxometry, variable temperature experiments, and chemical exchange spectroscopy, offer valuable data on ionic transport rates and pathways, thereby enhancing our understanding of battery performance at the microscopic level.[8−10]

Despite extensive reviews on the application of solid-state NMR in studying cathode materials, solid electrolytes, and various battery interfaces, NMR spectroscopic studies specifically focused on metal anodes have been relatively underexplored. This Perspective aims to address this gap by summarizing the recent advancements in solid-state NMR studies of metal anodes. We begin by exploring the fundamental origins of NMR signals and the critical effects of skin-depth and bulk magnetization in examining metallic samples. This foundation allows us to illustrate the quantitative capabilities of NMR in studying various metallic species, such as dendrites, mossy Li/Na, and inactive Li/Na, through carefully selected examples. We also delve into nucleus-based NMR methods for unraveling the complex composition of the solid electrolyte interphase (SEI). Finally, we examine how dynamic NMR methods can enhance our understanding of ion transport rates and pathways at the lithium metal/electrolyte interface, offering deeper insights into the material's morphology and chemistry

1.1. Origin of NMR Signals. The origin of Nuclear Magnetic Resonance (NMR) signals is rooted in the behavior of nuclei within a magnetic field. NMR capitalizes on the phenomenon of nuclear spin. The nuclear spin quantum number (I value) is a key parameter that determines whether a sample can produce observable signals. When the nuclear spin quantum number is zero ($I = 0$), these nuclei lack a corresponding magnetic moment, resulting in the absence of observable NMR signals. Fortunately, isotopes found in metal anodes typically possess nonzero spin quantum numbers ($I \neq 0$), exemplified by ^{6}Li ($I = 1$), ^{7}Li ($I = 3/2$), ^{23}Na ($I = 3/2$), *etc.* (Table 1),[11] making them ideal choices for NMR analysis. Furthermore, these nuclei often exhibit high natural abundance, enabling short acquisition times and a relatively high spectrum resolution. When coupled with isotope experiments, it facilitates investigations into the behavior of metal ion deposition/stripping and the tracking of ion transportation.[12]

Table 1. Concise Guide to Accessible Nuclei for Various Types of Metal Anodes

NMR isotope	Spin quantum number	Natural abundant (%)	Sensitivity	
			Relative sensitivity[a]	Absolute sensitivity[b]
^{6}Li	1	7.42	8.50×10^{-3}	6.31×10^{-4}
^{7}Li	3/2	92.58	0.29	0.27
^{23}Na	3/2	100	9.25×10^{-2}	9.25×10^{-2}
^{25}Mg	5/2	10.13	2.67×10^{-3}	2.71×10^{-4}
^{27}Al	5/2	100	0.21	0.21
^{39}K	3/2	93.1	5.08×10^{-4}	4.73×10^{-4}
^{41}K	3/2	6.88	8.40×10^{-5}	5.78×10^{-6}
^{67}Zn	5/2	4.11	2.85×10^{-3}	1.17×10^{-4}

[a]Under constant magnetic field or equal number of nuclei. [b]Product of relative sensitivity and natural abundance of isotopes.

Specifically, when a sample is placed in a strong external magnetic field, nuclear magnetic moments become aligned in space due to the Zeeman effect. The application of a specific radiofrequency (RF) pulse imparts energy to the nuclear magnetic moments, i.e., resonance, and then deviation from their equilibrium positions. After the cessation of the RF pulse, the excited nuclear magnetic moments spontaneously release energy at a specific frequency. This phenomenon is termed free induction decay (FID) and is responsible for generating the NMR signal (Figure 1a). By using a magnetic resonance detector, the signal produced during FID can be captured and analyzed.[8,13] The NMR signal carries valuable information about the nuclei present in the sample. It offers quantitative insights into the sample composition, provides details about the local structure of target ions, reveals the evolution of interfacial morphology, and offers dynamic information relevant to metal anodes.[6,9,14] It is essential to note that NMR spectroscopy utilizes electromagnetic waves with very long wavelengths (approximately $10^{6}-10^{9}$ μm), frequencies in the MHz range, and low-energy levels. This type of irradiation avoids inducing molecular vibration, rotational transitions, and electronic level transitions. Consequently, solid electrolyte interphases allow for nondestructive sample detection, proving particularly beneficial for electrochemical *in situ* characterization.[15,16]

1.2. Skin-Depth Effects in Metal Sample. The skin effects observed in NMR refer to a phenomenon where the RF magnetic field penetrates the sample in a nonuniform manner, but instead, its penetration is more pronounced near the surface. Understanding and effectively managing skin effects are crucial for obtaining accurate and reliable NMR spectra, especially in studies involving metal samples, where electrical conductivity plays a significant role. This nonuniformity penetration arises from the intricate interplay between the RF field and the electrical conductivity of the sample. The manifestation of skin effects stems from the concept of "skin depth", a quantification of the depth to which the RF field can permeate a material before experiencing a significant reduction in amplitude, typically reduced to 1/e (approximately 37%) of its surface value (Figure 1b).[13,17] The skin depth is influenced by several factors, including the electrical conductivity of the sample and the frequency of the RF field.

According to the principles of skin effects, delineating the behavior of the RF magnetic field ($\omega(x)$) within a bulk metal, it is observed that the RF field may undergo an exponential decay as a function of depth (x) as shown in eq 1.[15,18]

$$\omega(x) = \omega_1 e^{-x/d} \tag{1}$$

The skin depth (d) can be determined by the following, eq 2:[16]

$$d = \frac{1}{\sqrt{\pi \mu_0}} \sqrt{\frac{\rho}{\mu_r f}} \tag{2}$$

where μ_0 represents the permeability of vacuum, μ_r signifies the relative permeability of the metal, ρ denotes the resistivity of the metal, and f corresponds to the frequency of the applied RF field. For the metal anode, μ_r and ρ are associated with the intrinsic properties of the samples and are influenced by the temperature of the testing environment. Meanwhile, f represents the Larmor frequency of the sample in NMR, primarily dependent on the magnetic field strength and studied nuclei. Table 2 provides calculations of skin depth for various pure metal materials under varying magnetic field strengths, at a fixed temperature of 293 K. Though the depth is in the

https://doi.org/10.1021/acs.jpcc.4c05822
J. Phys. Chem. C 2024, 128, 18659−18677

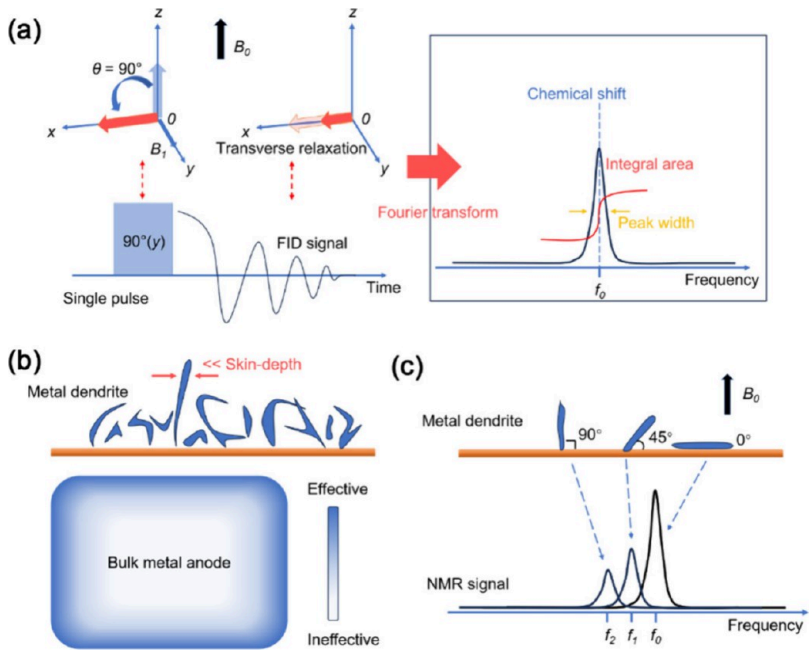

Figure 1. (a) Schematic diagram of source of nuclear magnetic signal, (b) schematic showing the radiofrequency penetration in a block of lithium metal and in the whiskerlike dendritic structures, and (c) bulk magnetic susceptibility effect on the ^{7}Li shift of lithium metal.

Table 2. Calculated Skin Depths of Different Nuclei for Various Types of Metal Anodes

				Skin depth (μm)		
Isotope	permeability of the vacuum (m kg A^{-2} s^{-2})	Relative permeability[19]	Resistivity (10^{-8} Ω m)[19]	400 M	600 M	800 M
^{6}Li	$4\pi \times 10^{-7}$	1.0000142	9.28	19.99	16.32	14.14
^{7}Li		1.0000142	9.28	12.31	10.04	8.70
^{23}Na		1.0000085	4.77	10.69	8.73	7.56
^{25}Mg		1.0000131	4.39	21.32	17.41	15.07
^{27}Al		1.0000165	2.65	8.03	6.55	5.68
^{39}K		1.0000208	7.2	31.27	25.53	22.11
^{63}Cu		0.9999945	1.68	6.34	5.17	4.48
^{67}Zn		0.9999908	5.9	24.45	19.96	17.28

micrometers level, the deposited metal in batteries always exhibited the porous and mossy type (1−2 μm), which enable the full penetration of RF frequency.[16] Only in this case is the signal from these metal microstructures directly proportional to their volume or mass, which lays the foundation for a quantitative analysis of metal anodes by NMR.

To mitigate the impact of skin effects, various strategies can be employed, such as optimizing the RF pulse sequence, adjusting the magnetic field strength (low magnetic field), raising the testing temperature appropriately, conducting isotope experiments (the skin-depth of ^{6}Li is nearly double that of ^{7}Li), or utilizing specialized NMR probes designed to minimize skin effects.

1.3. Bulk Magnetic Susceptibility Effects. When conducting NMR testing on metal electrodes, the bulk magnetic susceptibility (BMS) effects represent another critical factor that requires careful consideration. Specifically, when a sample is placed within a magnetic field, it generates a corresponding demagnetizing field based on the properties of the sample. This demagnetizing field is a complex entity influenced by various factors ranging from the micro- to macroscopic scale: (i) the intradipolar field originating from all paramagnetic ions within the Lorentz sphere; (ii) the demagnetization field produced by a specific crystallite, contingent upon the shape, orientation, and bulk magnetic susceptibility of the crystallite; (iii) the interdipolar field, calculated by summing up contributions from all crystallites across the entire sample, dependent on the overall sample shape.[20,21] The demagnetizing field alters the effective magnetic field experienced by the sample, ultimately resulting in changes in the chemical shift and peak broadening (Figure 1c).

It is evident that the fundamental cause of the BMS effects is the inherent heterogeneity within the sample, giving rise to diverse local magnetic fields experienced by distinct components (varied properties, arrangements/distributions, orientations, *etc.*), particularly in intricate multicomponent systems such as batteries, comprising components with distinct magnetic susceptibilities, including paramagnetic cathode materials, metallic anode materials, and diamagnetic electrolytes and separators.[22] Each component encounters the different local magnetic field. Among these components, the hierarchy of BMS impact follows diamagnetic < conductor < paramagnetic, primarily influenced by the presence of delocalized electrons in conductors and unpaired localized electrons in paramagnetic materials.[21,22] Additionally, interactions between different components can also induce alterations in the local magnetic field.[22]

https://doi.org/10.1021/acs.jpcc.4c05822
J. Phys. Chem. C 2024, 128, 18659−18677

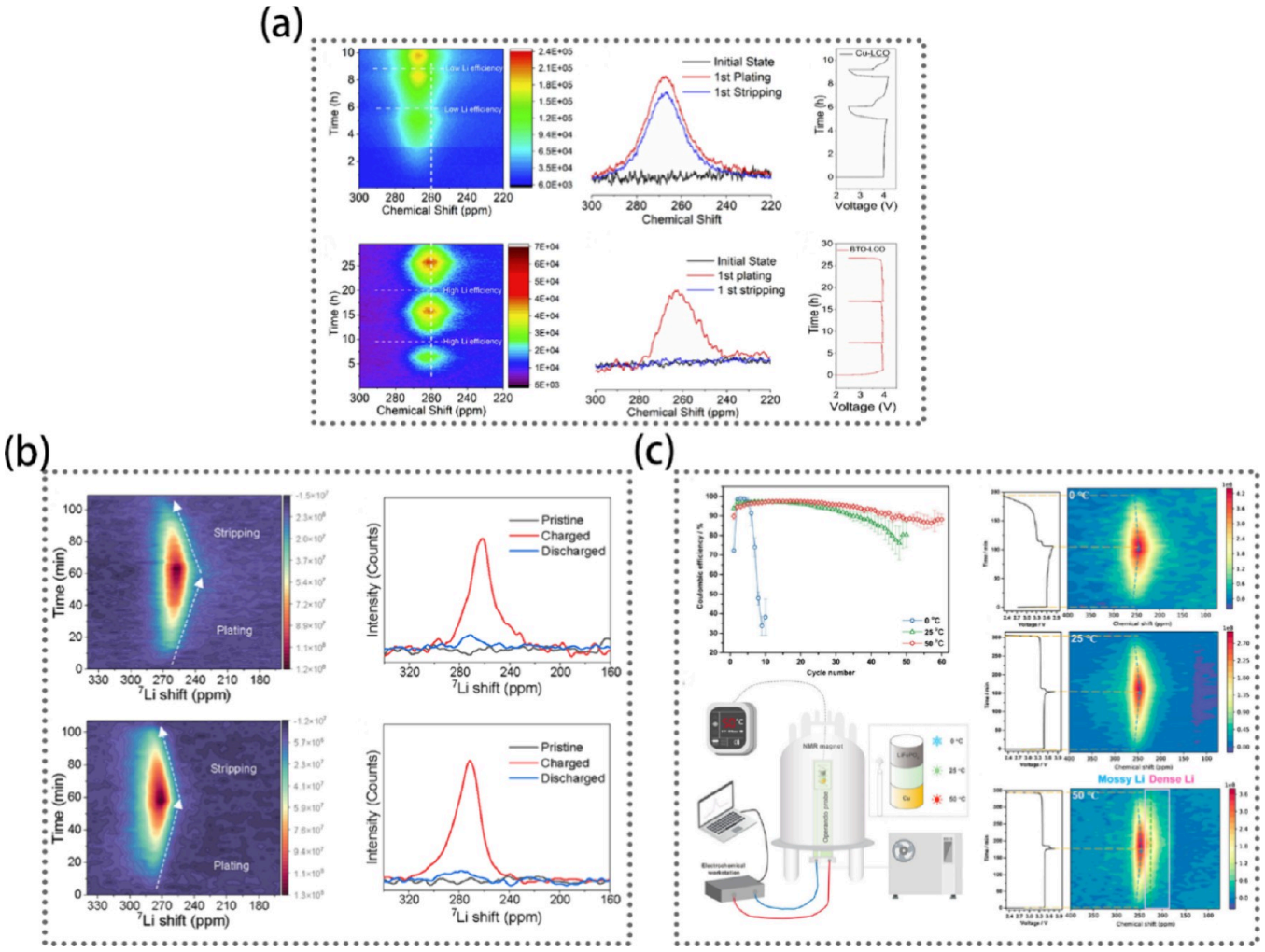

Figure 2. (a) Operando ^{7}Li solid-state NMR of Li metal plating/stripping on bare Cu and the BTO-coated Cu substrates in a full cell configuration. Reprinted with permission from ref 29. Copyright 2021 Springer Nature. (b) Operando ^{7}Li NMR spectra acquired during the first cycle of a Cu||LiFePO$_4$ cell using nanostructured Cu and regular Cu. Reprinted with permission from ref 30. Copyright 2022 American Chemical Society. (c) Variable-temperature operando NMR study of the microstructure evolution of the Li deposition/stripping process with 1 M LiODFB in EC/EMC electrolyte. Reprinted with permission from ref 23. Copyright 2023 American Chemical Society.

To alleviate the impact of the BMS effects, powder samples and magic-angle spinning (MAS) could be employed to mitigate orientation and anisotropic effects, respectively. However, metallic anodes typically exhibit a bulk form, and applying MAS to metallic materials poses challenges due to their high conductivity. This conductivity induces notable eddy currents and magnetic fields during MAS, potentially impacting the experimental sensitivity and stability. Additionally, heat generation is a consideration, as metallic samples undergoing MAS may encounter significant friction and induced currents, resulting in sample heating.

Fortunately, the internal NMR couplings in metallic materials mainly encompass chemical shift (electron shielding), knight shift (unpaired electrons), and dipolar coupling.[11] These interactions induce relatively modest chemical shifts and signal broadening, making metallic anodes well-suited for static NMR testing. Although the BMS effects may complicate NMR spectra under static conditions, a detailed analysis of the BMS effect could provide additional insights, for instance, discerning distinct microstructures at the metal anode interface based on variations in chemical shift[23−25] or adjusting the sample orientation in the magnetic field to modulate signals and improve the spectral resolution.[22]

1.4. NMR Measurements in Metal Anode Materials. Among various characterization techniques for battery materials, solid-state nuclear magnetic resonance (ss NMR) technology enables nondestructive testing of samples and possesses advantages such as quantitative and *in situ* analysis. It has become an indispensable tool in the study of the local structures of crystalline and amorphous battery materials. For metal anodes, ss NMR has been widely employed not only for quantitative and qualitative analysis of metal deposition/stripping evolution and solid electrolyte interphase (SEI) film on electrode surfaces but also for a thorough examination of ion transport between electrolyte/metal anode and SEI/metal anode interfaces, shedding light on the working and failure mechanisms.

1.4.1. Visualize and Quantify the Various Morphologic Metal Microstructures by In Situ NMR. Lithium/sodium metal is highly regarded as the most promising anode material for lithium and sodium batteries, boasting a remarkable theoretical specific capacity of up to 3860 mAh g^{-1} and 1165 mAh g^{-1}, respectively. In Li/Na metal batteries, the morphology of

https://doi.org/10.1021/acs.jpcc.4c05822
J. Phys. Chem. C 2024, 128, 18659−18677

deposited Li/Na metal greatly influences its reversibility, thus directly impacting the battery's cycling efficiency, lifespan, and safety performance. Given the air sensitivity and high reactivity of lithium and sodium metals, understanding the evolution of their deposition morphologies in a nondestructive way remains elusive. Key questions persist, such as how different factors, like cathode materials, electrolyte composition and concentration, separator and current collectors, applied pressure, and temperature, affect the morphology of deposited metal anode and how this morphology influences the reversibility of deposition/stripping. In lithium/sodium metal batteries, because of the BMS effect of Li/Na metal and significantly different chemical shifts between Li/Na metal and diamagnetic SEI species, NMR serves as a powerful technique to achieve the following objectives: (i) determine the deposition morphology evolution of lithium/sodium metal in an average manner, (ii) quantitatively analyze dead lithium/sodium metal and SEI in batteries, and (iii) distinguish metallic lithium/sodium from that lithium/sodium intercalation compounds (LiCx, NaCx) formed on other anode materials (such as graphite, hard carbon, and silicon) under fast charging or abusive conditions. The research content and our discussion of relevant literature have been presented in an upcoming review.

1.4.1.1. Visualize the Morphologic Metal Microstructure. As mentioned in the preceding theoretical section, the orientation of the metal sample with respect to the external magnetic field will influence its chemical shift, and the micrometer-scale skin depth is significantly larger than the nanoscale lithium/sodium dendrites, thus enabling the qualitative analysis of the various microstructure of the metal anode. Clare's group first employed the *in situ* ss NMR technique to quantitatively analyze the microstructure of lithium metal deposition. Bhattacharyya et al. found that the signal of lithium metal is directly proportion to the surface area other than the volume, evidenced by the skin-effect.[16] Assuming the surface area of the bulk lithium metal anode would not change significantly, the increased lithium metal NMR signals during cycling could be completely attributed to the formation of lithium metal microstructures. This method offers an opportunity to quantitatively understand the lithium metal microstructure, and its impact on the electrochemical performance could be obtained based on these quantitative data. In addition to the skin effect, the BMS effect gives the different chemical shifts of planar lithium metal and dendritic/mossy lithium metal. Trease et al. concreted the BMS effect by positioning a lithium metal strip in different angles with an external magnetic field of 0°, 30°, 45°, and 90° angles giving chemical shifts at 272, 265, 252, and 242 ppm, respectively, accompanied by observable signal broadening.[22] Furthermore, in a real lithium metal battery, varying the densification of deposited lithium metal by pressure, Chang et al. proposed that higher chemical shift (270 ppm) relates to the dendritic lithium metal while the lower one (−240 ppm) corresponds to the more uniform lithium metal. This work establishes the basement of *in situ* NMR in studying various metal microstructures.[25] And Chiou et al. noted that the polymer electrolytes with poor polymer segment compatibility exhibited higher chemical shifts and broader chemical shift distributions in ss NMR,[26] corresponding to relatively rough lithium deposition. Besides, *in situ* ^{7}Li NMR could be implemented to elucidate the impact of electrolyte composition or salt concentration on lithium deposition, specifically by altering SEI composition and interfacial ion transport properties.[17,27] Furthermore, researchers also stabilized lithium metal interfaces by constructing artificial SEI layers. Lennartz et al. found that highly cross-linked polyborosiloxanes (PBS) coatings on Li metal promoted more homogeneous lithium metal deposition with Li signal at lower chemical shifts (∼262 ppm) compared to less cross-linked PBS coatings (∼268 ppm).[28] For anode-free lithium metal batteries, the construction of suitable copper current collectors has been proven as an effective means of enhancing lithium metal deposition uniformity. For instance, *in situ* NMR studies on Cu||$LiCoO_2$ batteries with $BaTiO_3$ (BTO) coating on Cu foil demonstrated that high-dielectric scaffolds promote dense Li deposition and effective stripping due to the mitigated electric field gradients, resulting in minimal residual lithium after stripping (Figure 2a).[29] Moreover, altering the surface structure of copper current collectors is also demonstrated to effectively enhance lithium metal deposition coverage, achieving denser plating. Wang et al. further demonstrated through ^{7}Li NMR that lithium metal deposition on nanostructured copper current collectors tends to occur at lower ppm, corresponding to denser Li deposition (Figure 2b).[30]

Operation environment would also influence lithium deposition morphology in batteries, including the temperature and pressure. Studies employing variable-temperature operando ^{7}Li NMR measurements at 0, 25, and 50 °C reveal that compared to low/ambient temperatures, higher temperatures favor the formation of dense lithium deposition, reducing dead lithium formation (Figure 2c).[23] Additionally, experiments using *in situ* NMR setups capable of applying pressure indicate that lithium metal deposition gradually becomes denser under 0.5 MPa pressure, with almost no residual dead lithium after stripping.[31] Optimal pressure conditions are critical to promote dense deposition, while excessively low pressure or high pressure tends to result in lithium dendrite or mossy lithium metal formation. In addition to the external pressure, the pressure generated internally during battery cycling also affects the lithium deposition morphology. KüPers et al.[27] observed that the high-concentration electrolyte 3-TFSI-E (3 M LiTFSI in DME:DOL, 1:1) exhibited a higher peak at 268 ppm than 1-TFSI-E (1 M LiTFSI in DME:DOL, 1:1) at 266 ppm, suggesting lower density and needlelike lithium deposits in the high-concentration electrolyte. The lower ^{7}Li NMR chemical shift observed with the 1-TFSI-E electrolyte is attributed to increased internal pressure, resulting from continuous and inhomogeneous lithium deposits. This phenomenon could lead to the bending of needlelike lithium deposits and the coalescence of lithium microstructures during longer deposition times. It is worth noting that the ^{7}Li NMR spectra of cells with 1-TFSI-E exhibited similar features compared to those of 1-TFSI-C (1 M LiTFSI in EC:DEC (3:7)) with nearly constant peak intensity at 246 ppm and chemical shifts of 266 ppm or 267 ppm for lithium deposits. However, distinguishable morphological differences were observed in the scanning electron microscopy (SEM) images. Hence, it is imperative to acknowledge that diverse deposition morphologies may exhibit similar shifts, necessitating a combination of various characterization techniques, such as atomic force microscopy (AFM), SEM, among others, to thoroughly evaluate lithium metal deposition morphology.

In contrast to the easily separable solid−liquid interface in lithium batteries, the tight adhesion between the lithium metal and the solid electrolyte in solid-state batteries (SSBs) poses challenges in separating the solid−solid interface to obtain

https://doi.org/10.1021/acs.jpcc.4c05822
J. Phys. Chem. C 2024, 128, 18659−18677

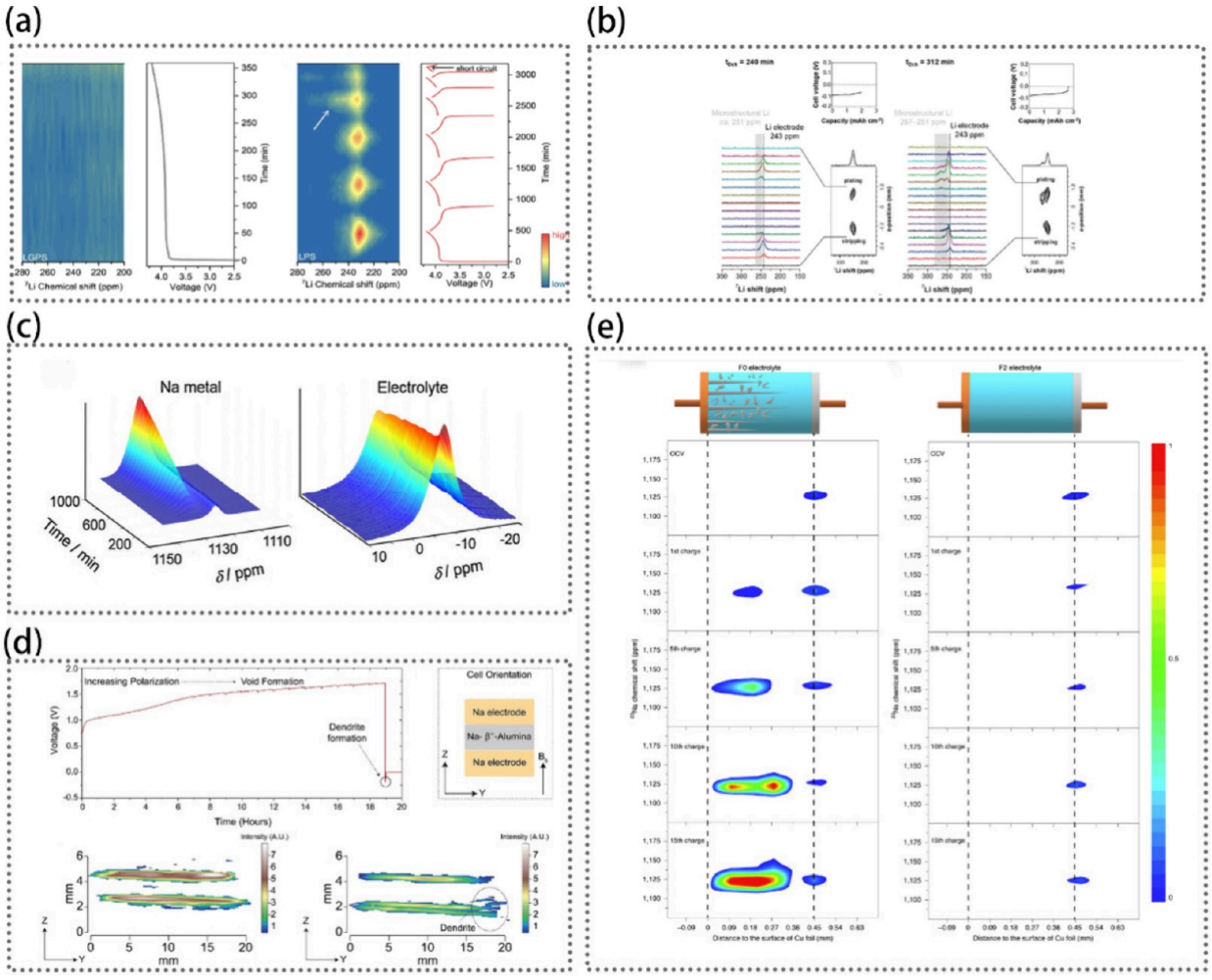

Figure 3. (a) Contour plots of operando ^{7}Li NMR spectra and the integral of the lithium metal signal versus time in anode-free batteries with different sulfide solid electrolytes. Reprinted with permission from ref 24. Copyright 2023 Springer Nature. (b) One-dimensional ^{7}Li NMR spectra as a function of z-position in ^{7}Li MRI of Li−LLZTO−Li symmetrical cells. Reprinted with permission from ref 34. Copyright 2019 American Chemical Society. (c) ^{23}Na *in situ* NMR spectra of the Na metal (left) and Na electrolyte (right) peaks during galvanostatic cycling. Reprinted with permission from ref 36. Copyright 2016 Elsevier. (d) Galvanostatic cycling and ^{23}Na MRI images of the Na | Na-β''-Alumina | Na cell. Reprinted with permission from ref 38. Copyright 2021 Wiley-VCH. (e) *In situ* ^{23}Na metal MRI images of the Na || Cu batteries. Reprinted with permission from ref 15. Copyright 2020 Springer Nature.

intact electrode interfaces. Therefore, *in situ* NMR is considered as a crucial characterization tool in SSBs, enabling nondestructive and real-time monitoring of the plating/stripping evolution at the buried interface. In sulfide SSBs, the continuous side reactions between sulfide solid electrolyte and Li metal would deteriorate the interface and the uniformity of lithium metal deposition. Compared to liquid electrolyte-based batteries, a more pronounced and well-resolved ^{7}Li NMR signal of lithium microstructure was observed by Liang et al. in sulfide SSBs.[24] Their results show that the ^{7}Li chemical shift (230 ∼ 240 ppm) in SSBs is lower than that in liquid electrolyte-based batteries (240 ∼ 275 ppm), possibly attributed to the synergistic effects of the delithiated cathode and the morphologies of deposited Li. For the $Li_7P_3S_{11}$(LPS)) solid electrolyte configuration, a distinct 270 ppm signal is observed in the fourth charge, potentially related to the growth of lithium dendrites into the LPS solid electrolyte (Figure 3a).

Because of the uneven morphology of lithium metal resulting from deposition and stripping processes, obtaining clear spatial information is crucial for understanding the underlying formation mechanisms of lithium microstructures. The development of magnetic resonance imaging (MRI) offers valuable spatial insights into the microscopic morphology of lithium metal.[32] Chang et al. utilized ^{7}Li chemical shift imaging to correlate the onset time of lithium dendrite formation with current density. Their work demonstrated the Sand model at high current densities and identified a separate model for low current densities.[33] Subsequently, ^{7}Li MRI was also employed to observed Li microstructural growth in Li-$Li_{6.5}La_3Zr_{1.5}Ta_{0.5}O_{12}$ (LLZTO)-Li all-solid-state symmetric cells, monitoring the evolution of Li dendrites through the solid electrolyte[34] (Figure 3b). However, direct MRI observation of dendrite growth through a relatively insensitive metal nucleus limits spatial and temporal resolution. Therefore, Jerschow et al. developed a 3D 1H MRI technique to visualize the microscopic growth of lithium metal via the dendrites' indirect effects on the surrounding electrolyte, significantly enhancing the sensitivity of MRI technology.[35]

The abundance and cost-effectiveness of sodium resources have sparked significant interest in sodium-based batteries, with sodium metal being recognized as an ideal anode material due to its high theoretical specific capacity and low operating

https://doi.org/10.1021/acs.jpcc.4c05822
J. Phys. Chem. C 2024, 128, 18659−18677

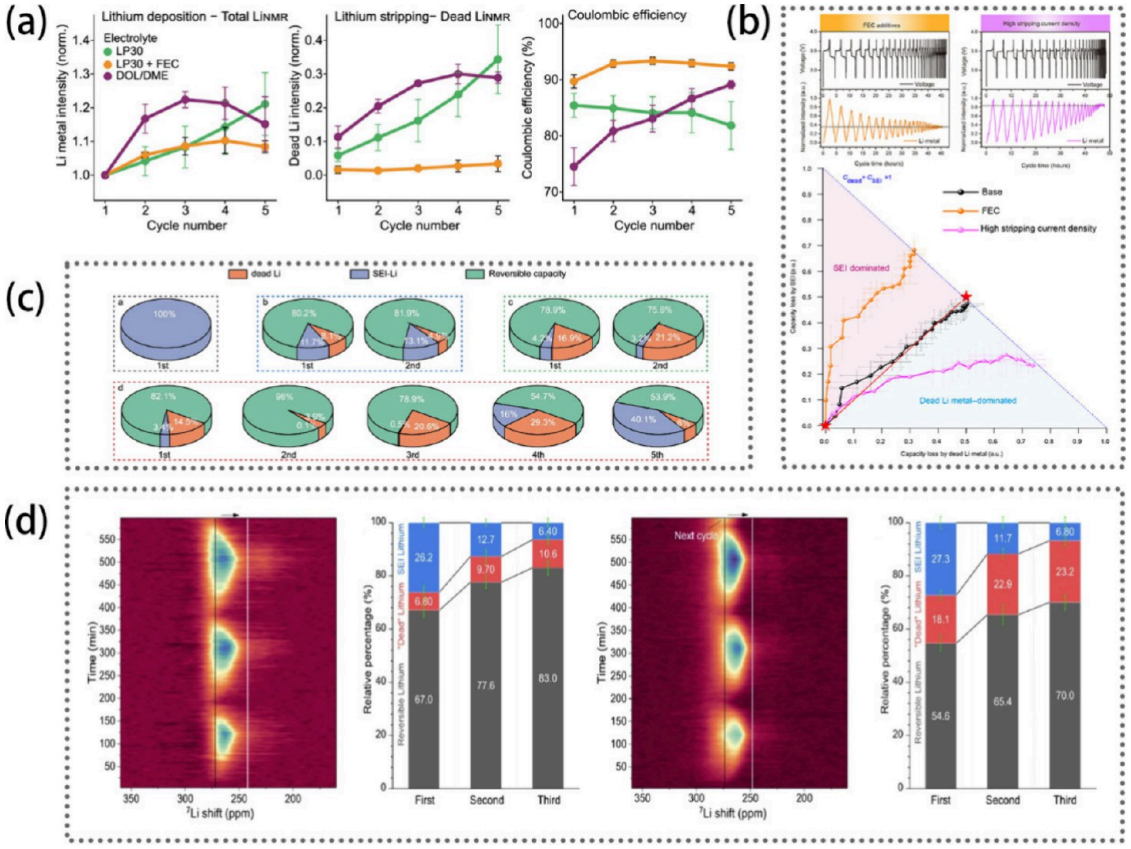

Figure 4. (a) Average value of total Li_{NMR} intensity at the end of plating and dead Li_{NMR} at the end of stripping and CE obtained from electrochemical cycling data. Reprinted from ref 40. Copyright 2020 American Chemical Society. (b) Operando NMR data and the normalized capacity loss due to SEI formation and dead Li metal under different conditions. Reprinted with permission from ref 42. Copyright 2021 The American Association for the Advancement of Science. (c) Quantitative analysis of operando ^{7}Li NMR spectra of SSBs with different sulfide solid state electrolytes. Reprinted with permission from ref 24. Copyright 2023 Springer Nature. (d) Operando ^{7}Li solid-state NMR spectra and quantification of the lithium species in different electrolytes. Reprinted from ref 30. Copyright 2022 American Chemical Society.

voltage. Since sodium metal is more active than lithium metal, the deposited sodium metal exhibits more complex morphologies during the deposition/stripping process. However, compared to lithium metal, research on sodium microstructures is considerably less extensive. Tracking the evolution of sodium metal microstructures over time presents challenges for conventional *ex situ* characterization methods, whereas *in situ* NMR offers real-time quantitative insights into the growth process. Na metal exhibits a larger Knight shift around 1130 ppm than Li metal due to the larger atomic volume and density of states at Fermi level.[18] Moreover, the orientation-dependent shift of sodium metal is smaller than that of lithium metal due to the smaller BMS effect of sodium metal than that of lithium metal. Hence, during *in situ* ^{23}Na NMR analysis of sodium deposition, the emergence of small shoulder corresponding microstructures can be observed, contrasting with the well-resolved signal observed in the lithium metal system. As reported by Pecher et al.,[36] an additional signal appears at 1133 ppm after approximately 1.5 h of galvanostatic plating, corresponding to the formation of Na microstructures, and this signal gradually grows with Na deposition time (Figure 3c). To enhancing the space-resolved capability, *in situ* ^{23}Na MRI has been used to study the spatial distribution of sodium microstructures during Na deposition/stripping cycles in liquid electrolyte system.[15,37] Xiang et al. proved that the continuous growth of the microstructure of sodium metals would lead to a linear increase in the deposition overpotential through *in situ* 23Na MRI and operando NMR techniques. Until a transition voltage of 0.15 V is reached, a violent electrochemical decomposition of the electrolyte is triggered, resulting in the formation of a mossy sodium micromorphology and rapid battery failure (Figure 3e).[15] Furthermore, Bruce's group employed *in situ* ^{23}Na MRI to observe the growth of dendritic sodium in solid-state symmetric cells with sodium metal and ceramic solid electrolytes. Since MRI cannot image crack development in solid-state batteries, they further combined this with X-ray computed tomography to track morphological changes in the solid-state cells (Figure 3d).[38] The above studies demonstrate the outstanding advantages of NMR in characterizing microstructural features, including qualitative, nondestructive, *in situ* detection, and holistic material characterization rather than regional analysis, thereby providing robust support for elucidating the working mechanisms of metal anodes and validating the effectiveness of modification strategies.

1.4.1.2. Quantify the Dead Lithium Metal. In addition to the microstructure formation that may potentially lead to short circuit, the uneven stripping process would produce lithium metal isolated from current collectors, resulting in the formation of dead lithium metal. The dead lithium metal can lead to the loss of lithium inventory and increase safety issues as it is still chemically active lithium metal. Quantifying the dead Li could help us to evaluate the residual active lithium and further predict the cycle-life of lithium metal batteries. As

https://doi.org/10.1021/acs.jpcc.4c05822
J. Phys. Chem. C 2024, 128, 18659−18677

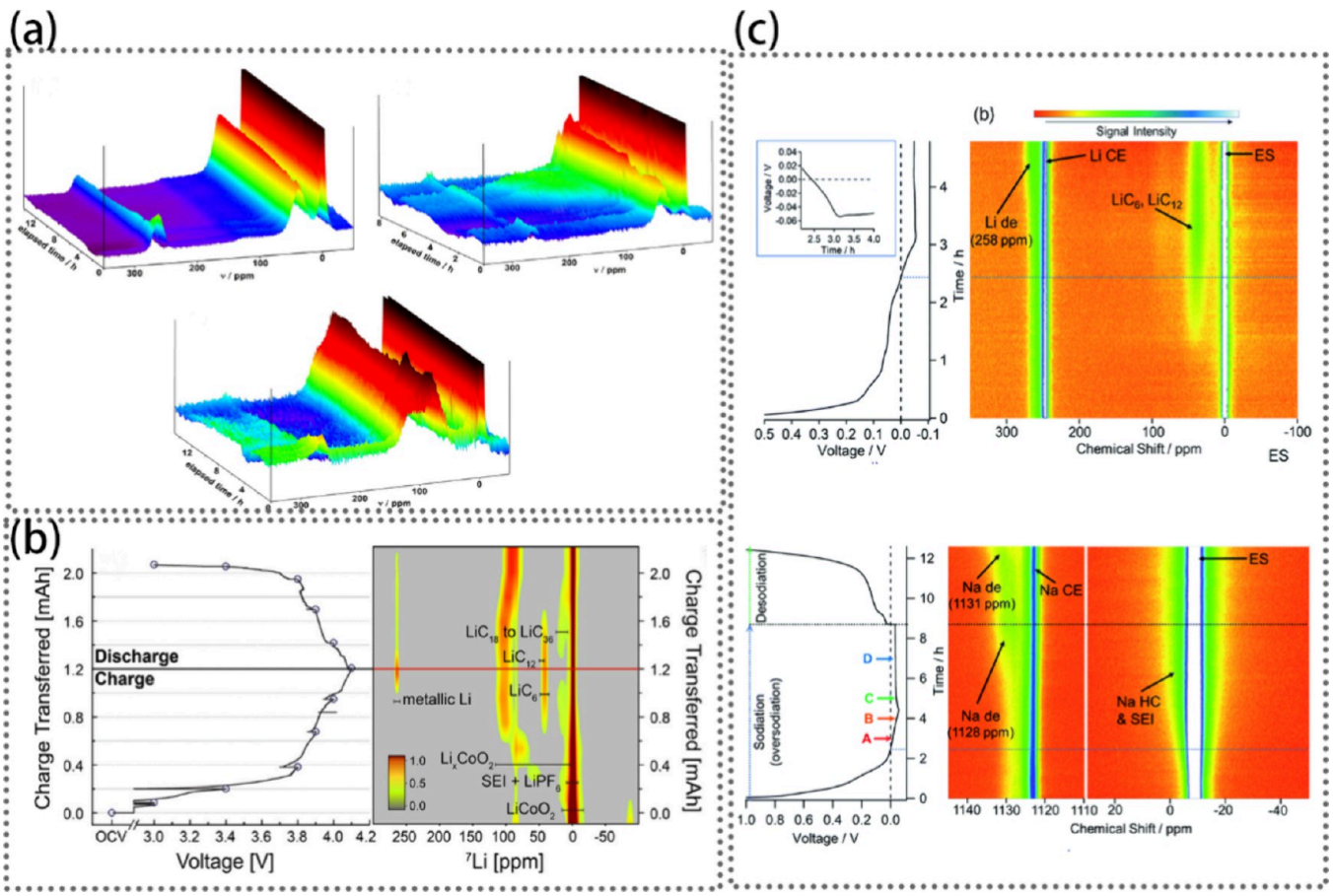

Figure 5. (a) Temporal variations of ^{7}Li NMR spectra of LCO-graphite, NCA-graphite, and LCO-hard carbon cells after overcharging. Reprinted with permission from ref 45. Copyright 2014 Elsevier. (b) Electrochemical profile and *in situ* MAS ^{7}Li NMR spectra of $LiCoO_2$/graphite jelly roll cell. Reprinted with permission from ref 52. Copyright 2019 American Chemical Society. (c) Electrochemical profile and operando ^{7}Li NMR spectra of graphite anode during lithiation and hard carbon anode during oversodiation and desodiation. Reprinted with permission from ref 51. Copyright 2020 Royal Society of Chemistry.

an uneven stripping product of metal microstructures, the nanoscale of dead lithium/sodium metal can be fully penetrated by RF frequency, enabling its capability in quantifying. Initially, the first attempt was in Li||Cu batteries.[39] However, since both lithium metal counter electrode and dead Li metal on the copper would generate NMR signals, it was necessary to further employ *ex situ* ^{7}Li NMR to distinguish the dead lithium signals from the lithium metal signals. Nonetheless, combining *in situ* and *ex situ* NMR may introduce errors due to material loss during *ex situ* sampling. For example, the dead lithium metal free in the electrolyte cannot be detected by this *ex situ* method. In contrast, using *in situ* batteries with LFP||Cu configuration effectively avoids signal interference from lithium metal. The lithium metal resonance signals in NMR spectra corresponded well to variations in deposited lithium metal on the Cu foil during the deposition and stripping processes. In 2020, Gunnarsdóttir et al. conducted a study using NMR measurements and Coulombic efficiency (CE) to quantify the formation of inactive dead lithium and SEI in Cu||$LiFePO_4$ cells (Figure 4a).[40] They investigated the relative formation rates of dead lithium and SEI in carbonate- and ether-based electrolytes and revealed that electrochemical SEI formation contributed more to capacity losses in the anode-free battery compared to dead lithium formation. This contrasts with Fang's titration gas chromatography (TGC) results,[41] which suggested that dead lithium was the primary factor in capacity losses during the first cycle and subsequent cycles. Gunnarsdóttir et al. attributed this discrepancy to differences in the battery systems studied (Li||Cu cells in Fang's work). In the meantime, Xiang et al. also found that in Cu||$LiFePO_4$ batteries, the formation of the SEI was more pronounced during the initial cycles than the formation of dead lithium through *in situ* NMR analysis (Figure 4b).[42] Thus, they deeply explored discrepancies in analyzing dead lithium components using NMR quantitative techniques, TGC, and mass spectrometry titration (MST), attributing this discrepancy to the presence of lithium hydride (LiH) and highlighting the TGC method's limitations in independently quantifying dead lithium due to its neglect of LiH presence. Besides, for certain battery systems like SSBs in which the lithium metal/electrolyte interface is obscured, destructive titration methods may struggle to offer precise results. Hence, NMR should be deemed a more suitable tool for quantifying inactive lithium during cycling than other methods. In anode-free lithium cells with various sulfide solid electrolytes, *in situ*/*ex situ* NMR was employed to quantitatively characterize dead lithium, reversible lithium, and SEI components, providing a comprehensive understanding of their failure mechanisms. For example, SEI lithium formation was more significant than dead lithium formation in LSiPSCl cells. Conversely, in LPS cells, dead lithium predominantly contributed to capacity loss initially, with subsequent cycles witnessing larger SEI

https://doi.org/10.1021/acs.jpcc.4c05822
J. Phys. Chem. C 2024, 128, 18659−18677

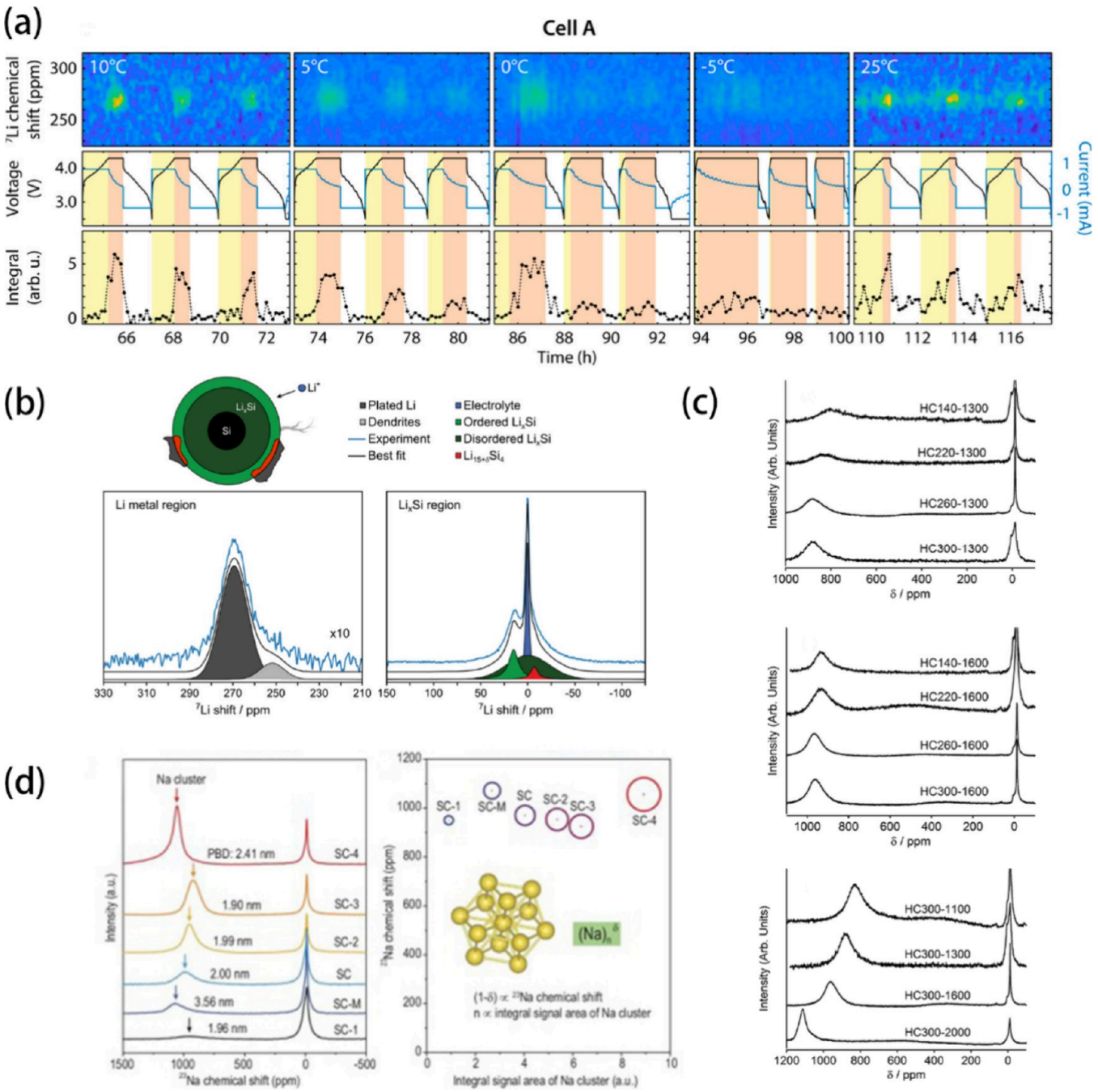

Figure 6. (a) Operando NMR spectrum of Li metal deposition in NMC811/graphite full-cells operating at different temperatures. Reprinted with permission from ref 53. Copyright 2020 American Chemical Society. (b) Deconvolution of a ^{7}Li NMR spectrum at the top of charge (TOC) after charging the Si||LiNi$_{0.6}$Mn$_{0.2}$Co$_{0.2}$O$_2$ cell at a rate of 2C. Reprinted with permission from ref 46. Copyright 2023 American Chemical Society. (c) ^{23}Na NMR spectra of fully sodiated hard carbon samples prepared by dehydration and carbonization at different temperatures. Reprinted with permission from ref 56. Copyright 2019 Elsevier. (d) *Ex situ* ^{23}Na ss NMR spectra of different hard carbon samples at 0.005 V for the first discharge and ^{23}Na chemical shift versus integral signal area of Na clusters for different hard carbon samples. Reprinted with permission from ref 58. Copyright 2022 Oxford University Press.

formation (Figure 4c).[24] On the basis of the quantitative analysis advantages of NMR, Wang et al. employed operando ^{7}Li NMR to study the evolution of lithium microstructure and quantify lithium species postfirst cycle in Cu||LiFePO$_4$ cells with varying electrolyte concentrations[30] or high entropy (HE) electrolytes.[43] Higher electrolyte concentrations were found to promote the formation of columnar lithium deposition with enhanced reversibility, as evidenced by a reduced percentage of lithium species in the SEI and decreased presence of "dead" lithium (Figure 4d), while the HE electrolyte demonstrated reduced dead lithium formation and promoted the formation of a thinner and inorganic-rich SEI. In short, *in situ*/*ex situ* NMR techniques have been employed to quantitatively analyze the evolution of SEI and dead lithium in liquid and solid-state lithium metal batteries during long-term cycling, aiding in the exploration of battery failure mechanisms. However, it is crucial to note that the ability of NMR to quantify lithium metal is also influenced by the skin effect, particularly when

https://doi.org/10.1021/acs.jpcc.4c05822
J. Phys. Chem. C 2024, 128, 18659−18677

dealing with large deposition areas. Caution should be exercised in such cases.

1.4.1.3. Detect the Lithium Plating in Other Anode Substrates. For lithium-ion batteries utilizing other anode materials (such as graphite, hard carbon, and silicon), battery operation relies on the reversible intercalation and deintercalation of Li^+ ions in the electrode materials. Consequently, the irreversible loss of active lithium during battery cycling is a key factor contributing to battery degradation. However, in long-term cycling or under abusive conditions (such as overcharging and low temperature), lithium plating and the formation of dead lithium may occur in lithium-ion batteries, leading to battery capacity degradation and posing safety concerns due to the potential for internal short circuits. Quantifying lithium compounds and dead lithium in carbon/silicon anodes of batteries nondestructively has been challenging. In NMR spectra, graphite intercalation compounds (GIC) typically appear around 40 ppm,[44] while signals from lithiated hard carbon anodes are observed between ∼40−140 ppm.[45] Besides, the silicon intercalation (Li_xSi) peaks are located at chemical shifts between −50 and 50 ppm.[46] These Knight shifts are distinctly different from plated Li metal (∼250 ppm), enabling separate monitoring of intercalation and plating processes in carbon/silicon anodes using *in situ* NMR. Since the lithium plating layer on carbon anodes is thinner than the skin depth, radiofrequency fields can fully penetrate it. Consequently, *in situ* and *ex situ* NMR can quantitatively or semiquantitatively analyze irreversible lithium losses in lithium-ion batteries, revealing degradation mechanisms.[47,48] *In situ* NMR reveals that when the battery is overcharged, carbon anodes (graphite and hard carbon) accumulate metallic lithium on their surfaces (Figure 5a).[45] This active dendritic lithium undergoes oxidation and reinsertion into the anode within hours, known as the relaxation effect.[44] Hard carbon anodes exhibit a more pronounced relaxation effect due to their porous and bufferable structure.[45] Further research indicates that lithium deposition on carbon anodes is influenced by the temperature and cycling protocols. Lower temperatures lead to increased lithium deposition on the carbon anode, observed through rising lithium metal resonance signals in the *in situ* NMR spectra. However, cycling under pulse current mode at low temperatures does not induce lithium plating.[49] The sensitivity of NMR to the metal orientation relative to the static magnetic field allows for distinguishing different forms of lithium deposition on graphite and silicon anodes (Figure 6b).[46,50] Utilizing this feature and designing highly sensitive parallel plate NMR resonators enable differentiation of lithium deposits on the anode surface, including lithium dendrite and partly reversible lithium films. Additionally, integrating *in situ* NMR spectra with electrochemical curves in Lill|carbon anode batteries could accurately determine the onset of lithium plating.[51] Research shows that in graphite anodes, the formation of lithium dendrites at 258 ppm chemical shift begins shortly after or immediately following the minimum potential in the lithiation curve. Conversely, in hard carbon anodes, quasi-metallic lithium clusters form first, followed by the appearance of lithium dendrite signals after cluster formation, and a similar scenario is observed in hard carbon sodiation processes (Figure 5c).[51]

Due to the limited resolution of static *in situ* NMR experiments, which cannot finely resolve the broad graphite lithiation signal around 40 ppm, Freytag et al.[52] devised a novel *in situ* Magic Angle Spinning (MAS) ^{7}Li NMR strategy using a $LiCoO_2$/graphite jelly roll cell design (Figure 5b). This approach effectively enhances spectral resolution, capturing signals from the battery's cathode, negative SEI, various lithiated graphite products, and lithium metal plating. On the basis of this full-cell *in situ* NMR, changes in both electrodes during charge and discharge processes can be monitored. However, in full-cell setups, various factors like different chemical shifts of multicomponent materials, changes in material properties (such as magnetization and conductivity) during cycling, and signal broadening caused by paramagnetism can interfere with experiments. The use of automatic tuning devices can overcome significant chemical shift offsets and peak broadening in materials with strong paramagnetism during charge and discharge processes.[36] Märker et al. used an automatic tuning device to collect *in situ* ^{7}Li signals of a high-paramagnetic cathode NCM811|| graphite full-cell battery during charging and discharging (Figure 6a).[53] They differentiated between cathode and anode signals based on distinct T1 relaxation times of the electrode materials and found batteries cycled at low temperatures exhibited lithium metal deposition at room temperature, possibly due to SEI accumulation and blockage of graphite pores formed at low temperatures. Additionally, due to strong interactions between ^{7}Li and conduction electrons, selective enhancement of lithium metal surface ^{7}Li nuclear magnetic resonance (NMR) signals can be achieved via the Dynamic Nuclear Polarization (DNP) technique.[54]

In sodium-ion battery systems, the hard carbon anode undergoes sodium intercalation at low voltages, gradually transitioning to metallic sodium. When the pores in hard carbon are sufficiently large, large quasi-metallic sodium clusters form within these pores.[55] This phenomenon manifests as higher chemical shifts in the NMR spectra compared with sodium-intercalated compounds. The sodium metallization properties of hard carbon materials vary under different synthesis conditions, including dehydration and carbonization temperatures,[56] and template strategies.[57] With an increasing synthesis temperature, the chemical shifts of sodium metal clusters gradually shift to higher values. Hard carbon prepared at a carbonization temperature of 2000 °C exhibits sodium cluster chemical shifts almost identical to metallic sodium (1130 ppm) (Figure 6c).[56] The formation of sodium metal clusters in hard carbon is highly influenced by the properties of hard carbon. Specifically, Li et al. extensively discussed the factors affecting sodium cluster formation, chemical shift, and integral area in carbon anode materials using high-resolution MAS NMR (Figure 6d).[58] The results indicate that the pore entrance diameter (PED) plays a role in cluster formation, with a smaller PED facilitating cluster formation outside pores, thus protecting the active pore surface. Larger pore body diameters (PBD) are associated with higher chemical shifts, indicating a greater sodium ion transfer charge. Additionally, the integrated signal area of sodium clusters is directly proportional to the number of probed nuclei, increasing with specific surface area (SSA) and thereby enhancing the cluster count and platform capacity. Compared to pure metal anodes, carbon/silicon anodes offer a wider array of structural parameters on composition and microstructure. The intricate interplay of these parameters, alongside modifications in electrode cycling conditions, results in rich features observed in NMR. Therefore, the analysis of NMR signals combined with their electrochemical properties can provide insights into the rational design of anode materials.

https://doi.org/10.1021/acs.jpcc.4c05822
J. Phys. Chem. C 2024, 128, 18659−18677

1.4.2. Clarify the Complex Chemical Composition of SEI by Multinuclear NMR. In lithium/sodium metal batteries, the solid electrolyte interphase (SEI) not only acts as a protective barrier against continuous electrolyte decomposition but also facilitates lithium-ion transport. Therefore, understanding the composition and distribution of the SEI has been a key focus in battery research. Despite the high reactivity and complexity of SEI layers on lithium/sodium metal anodes, which encompass both crystalline and amorphous components and are prone to instability in the presence of air and moisture, *in situ* and *ex situ* NMR techniques can be competent for quantitative and nondestructive analysis of SEI component. The SEI layer primarily consists of chemical and electrochemical reduction/oxidation products of electrolyte solvents, salts, and additives. It comprises both inorganic and organic components, with inorganic components predominantly detected by $^{6/7}$Li, ^{19}F, ^{31}P, and ^{23}Na NMR, while organic components are mainly detected by ^{1}H, ^{13}C, and ^{17}O NMR. Table 3 provides an overview of the chemical shifts of key SEI components in Li/Na metal batteries. This upcoming review will further outline the specific applications of ss NMR techniques in characterizing SEI components.

Table 3. Common Li/Na SEI Species and Corresponding Chemical Shift

Species	^{7}Li	Species	^{23}Na
Li_2O	2.8	Na_2O	55.1
LiOH	∼1	NaOH	21
Li_2CO_3	0	Na_2CO_3	7,7.5,-4
LiF	−1	NaF	7.2
LiCl	−1.1	NaCl	7.2
LiH	∼0.2	NaH	18.8
Li_2S	2.2	Na_2S	49.8
Li_3N	7.45	Na_3N	–
Li_2O_2	1.33	Na_2O_2	6.9, 11.8
Li_3PO_4	∼0	Na_3PO_4	10

Due to the high sensitivity and prevalence, ^{7}Li NMR is commonly utilized for qualitative and quantitative analysis of lithium-containing compounds in the SEI, such as LiF and Li_2O. However, due to the complexity of SEI components, spectra often exhibit broad peaks, prompting the use of higher-resolution isotope nuclei like ^{6}Li MAS NMR for analysis. ^{6}Li MAS NMR was used by Qian et al. to analyze the inorganic composition of the Li-containing SEI layer on the Cu current collector in a 4.0 M LiFSI/DME electrolyte after cycling (Figure 7d).[59] The fitting results of ^{6}Li MAS NMR spectra, ranging from −10 to + 10 ppm indicated the presence of LiF, Li_2S, Li_2O, and a small amount of LiFSI salt. Combined with ^{19}F MAS NMR and ^{6}Li MAS NMR spectra, Wan et al. detected various lithiated species in SEI layers derived from LiFSI-DME electrolytes with different concentrations and 3 M LiTFSI-DME electrolyte (Figure 7a).[60] The results show that the SEI from high-concentration electrolytes exhibited a significant presence of LiF. However, LiF was not detected in the SEI from 1 M LiFSI-DME. Such inorganic compounds contribute to enhancing the ionic conductivity and mechanical stability of the SEI layer, thereby improving battery cycling efficiency. In sulfide solid-state battery systems, the narrow electrochemical stability window of sulfide electrolytes makes them prone to oxidation and reduction. Characterizing the interface side reaction products of lithium metal/$Li_{10}SnP_2S_{12}$ (LSPS) electrolyte after cycling using *ex situ* ^{7}Li MAS NMR reveals the presence of Li_2S and Li_3P, elucidating the reasons behind the increased interfacial impedance.[61] However, due to the limited amount of the SEI layer and the restricted ^{7}Li chemical shift range of diamagnetic SEI species, directly distinguishing between different Li-containing components through a $^{6/7}$Li MAS NMR measurement is still challenging in some situations. Therefore, Hope et al. conducted lithium metal-transferred electrons for room temperature DNP testing, avoiding SEI composition changes. Microwave irradiation boosts nuclear polarizability, enhancing ^{7}Li, ^{1}H, and ^{19}F NMR signals at the SEI/lithium metal interface (Figure 7b).[62] Recently, Zhang et al. addressed this issue by employing cross-polarization (CP) ss NMR experiments to elucidate the chemical components and distribution within the SEI.[63] The SEI peaks were deconvolved by combining the fitting of CP ss NMR spectra of ^{1}H→^{7}Li (Li near H), ^{19}F→^{7}Li (Li near F), and a one-pulse measurement of bulk Li_2O. The analysis revealed that the SEI formed at a plating current density of 2 mA cm^{-2} showed the smallest amount of Li_2O, while the SEI formed at 5 mA cm^{-2} exhibited a higher proportion of amorphous LiF.

Organic components in the SEI are more challenging to characterize compared to inorganic components due to their amorphous nature. Nevertheless, ^{1}H and ^{13}C NMR can be utilized to analyze the organic components of SEI. Through comparative analysis of ^{6}Li, ^{19}F, ^{13}C, and ^{1}H MAS NMR spectra, Wan et al. discovered that the SEI formed in the 4 M LiFSI-DME electrolyte contained more lithiated species and exhibited higher density compared to those formed in the 1 M LiFSI-DME and 3 M LiTFSI-DME systems.[60] May et al. conducted quantitative characterization of insoluble SEI components in electrolytes with and without 0.10 M KPF_6 additive through ^{13}C ss NMR experiments.[64] Their results revealed increased polycarbonate (∼161 ppm) and organofluoride content in SEI with K^+ addition, along with reduced SEI thickness and solubility. Quantification of ^{1}H-^{13}C CPMAS ss NMR spectra further indicated a 20% decrease in the overall SEI content with 0.10 M KPF_6 addition. Girard et al. used ^{31}P, ^{7}Li, and ^{19}F MAS NMR to characterize the SEI layer formed in P111i4FSI ionic liquid electrolytes, providing an understanding on the composition and structure of the SEI (Figure 7c).[65]

Similar to lithium battery systems, the Na-containing SEI composition in sodium battery systems can be analyzed by tuning the ^{23}Na NMR. ^{23}Na 3Q-MAS NMR analysis by Cao et al. revealed that a significant portion of NaOH and Na_2S forms in the SEI layer when using a 4 M NaFSI-DME electrolyte, effectively passivating the surface of sodium metal during cycling.[66] Gao et al. discovered that sodium-difluoro(oxalato)-borate (NaDFOB) carbonate electrolytes exhibit excellent compatibility with sodium metal batteries. And their ^{23}Na and ^{11}B NMR results revealed that the SEI layer mainly consists of sodium diborate ($Na_4B_2O_5$), sodium tetrafluoroborate ($NaBF_4$), and carbonate (Na_2CO_3) during the initial cycle.[67] ^{23}Na MAS NMR was also utilized to monitor the evolution of SEI components on the surface of sodium metal in response to superconcentrated ionic liquid with varying water concentrations in the work of Ferdousi et al.,[68] revealing that the addition of water significantly influenced SEI formation, with approximately 1000 ppm of water promoting the development of a more uniform SEI. This SEI is primarily composed of NaF (7.4 ppm), metal oxides (Na_2O, 55 ppm), and complexes

https://doi.org/10.1021/acs.jpcc.4c05822
J. Phys. Chem. C 2024, 128, 18659−18677

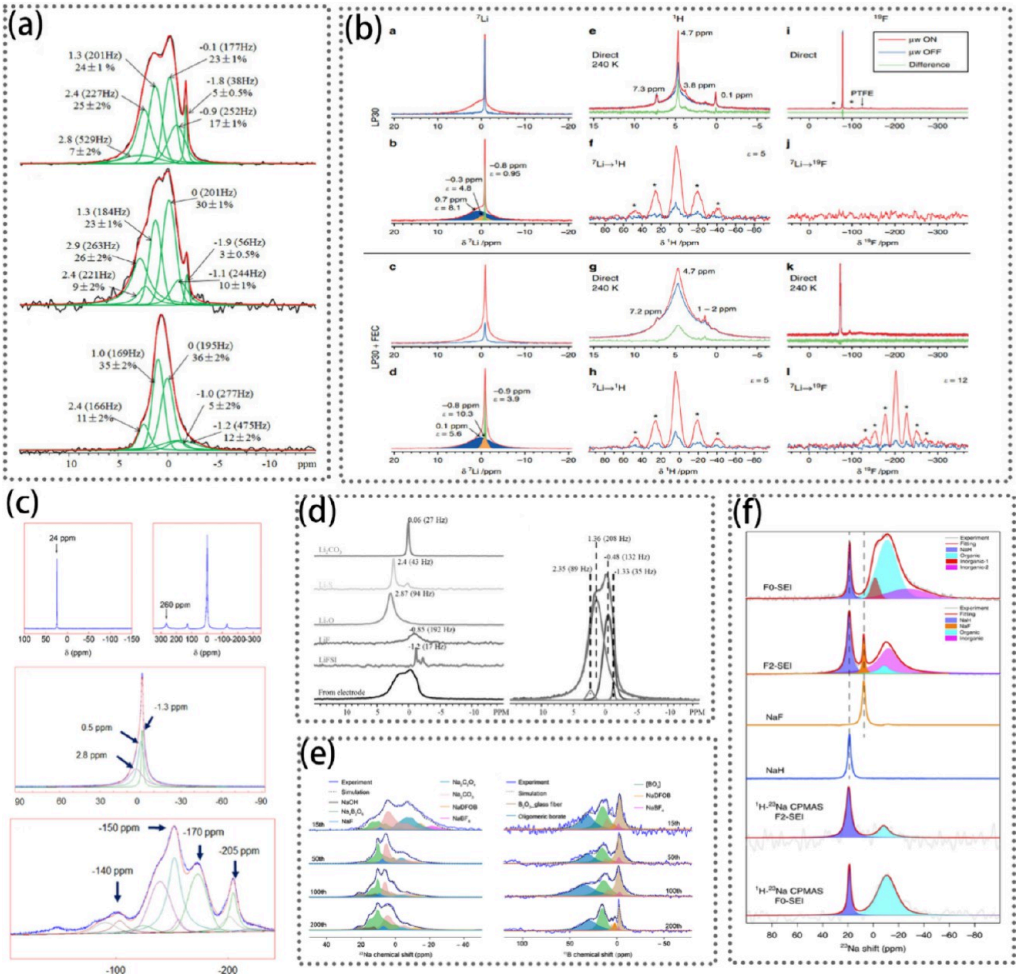

Figure 7. (a) Deconvolutions of the ^{6}Li NMR spectra for the SEIs harvested from CulLi batteries with 4 M LiFSI−DME, 1 M LiFSI−DME, and 3 M LiTFSI−DME as electrolyte. Reprinted from ref 60. Copyright 2017 American Chemical Society. (b) Selective enhancement of the SEI by Li metal DNP. Reprinted with permission from ref 62. Copyright 2020 Springer Nature. (c) ^{31}P NMR spectra, ^{7}Li NMR spectra, ^{7}Li NMR spectra with fitted peaks and ^{19}F NMR spectra with fitted peaks for the 50:50 (wt %) mixture of SEI deposit: alumina powder. Reprinted from ref 65. Copyright 2018 American Chemical Society. (d) ^{6}Li MAS NMR spectra of the residues formed on the Cu substrate recovered from a cell with 4.0 M LiFSI/DME electrolyte. Reprinted with permission from ref 59. Copyright 2016 WILEY-VCH. (e) ^{23}Na and ^{11}B ss NMR spectra of SEI species harvested from the Na metal surface after different cycles. Reprinted with permission from ref 69. Copyright 2022 The American Association for the Advancement of Science. (f) Single-pulse ^{23}Na NMR and ^{1}H → ^{23}Na CPMAS NMR spectra of SEI species harvested from Cu foil after 50 cycles and the reference spectra of NaF and NaH. Reprinted with permission from ref 15. Copyright 2020 Springer Nature.

(−12.6 ppm) associated with Na, FSI, and water molecules. The limited quantity and compositional complexity of the SEI formed in batteries make it difficult to fully elucidate the true and complete components of the SEI. Early on, due to limitations in characterization techniques, some highly reactive components within the SEI are overlooked. Because of the high sensitivity of ^{23}Na ss MAS NMR, some elusive materials have been validated recently. For instance, Xiang et al. found unexpected NaH (18.8 ppm) in the surface species obtained from cycled Cu foil in sodium metal batteries[15] (Figure 7f).

In addition to ^{23}Na NMR, *in situ* ^{1}H, ^{19}F, and ^{11}B NMR were also employed by Gao et al. to monitor the degradation of electrolyte comprising sodium difluoride (oxalate) borate (NaDFOB) and carbonate solvent in sodium metal batteries.[69] Chemical changes in the SEI components at various cycles were elucidated through ss NMR and XPS depth profiling (Figure 7e). The characterization revealed a gradual reduction of the DFOB anion, leading to the formation of a SEI layer rich in borate and fluoride.

1.4.3. Trace Li^{+} Exchange Dynamics in Lithium Metal Batteries at the Metal/Electrolyte Interface. Further analysis of the dynamic processes on the surface of lithium/sodium metal anodes is beneficial for a deeper understanding of the Li/Na ion transport at the electrode interface. However, the complexity of the reaction of multiphase components in batteries and the high activity of SEI and lithium/sodium metal have brought great difficulties to the study of interfacial dynamics. After decades of development, NMR techniques could directly probe ion exchange and diffusion kinetics at the interfaces of Li metal/electrolyte and Li metal/SEI by conducting the cross-polarization, isotope tracing, two-dimensional exchange spectrum, and other NMR experiments. Here, we summarize representative research studies in the literature on the application of NMR for analyzing the interfacial dynamics of metal anodes.

By conducting isotope exchange experiments, NMR can be employed to probe ion exchange processes at the electrode/electrolyte interface. Ilott et al. investigated lithium-ion exchange at the natural abundance ^{7}Li electrolyte-^{6}Li-enriched

https://doi.org/10.1021/acs.jpcc.4c05822
J. Phys. Chem. C 2024, 128, 18659−18677

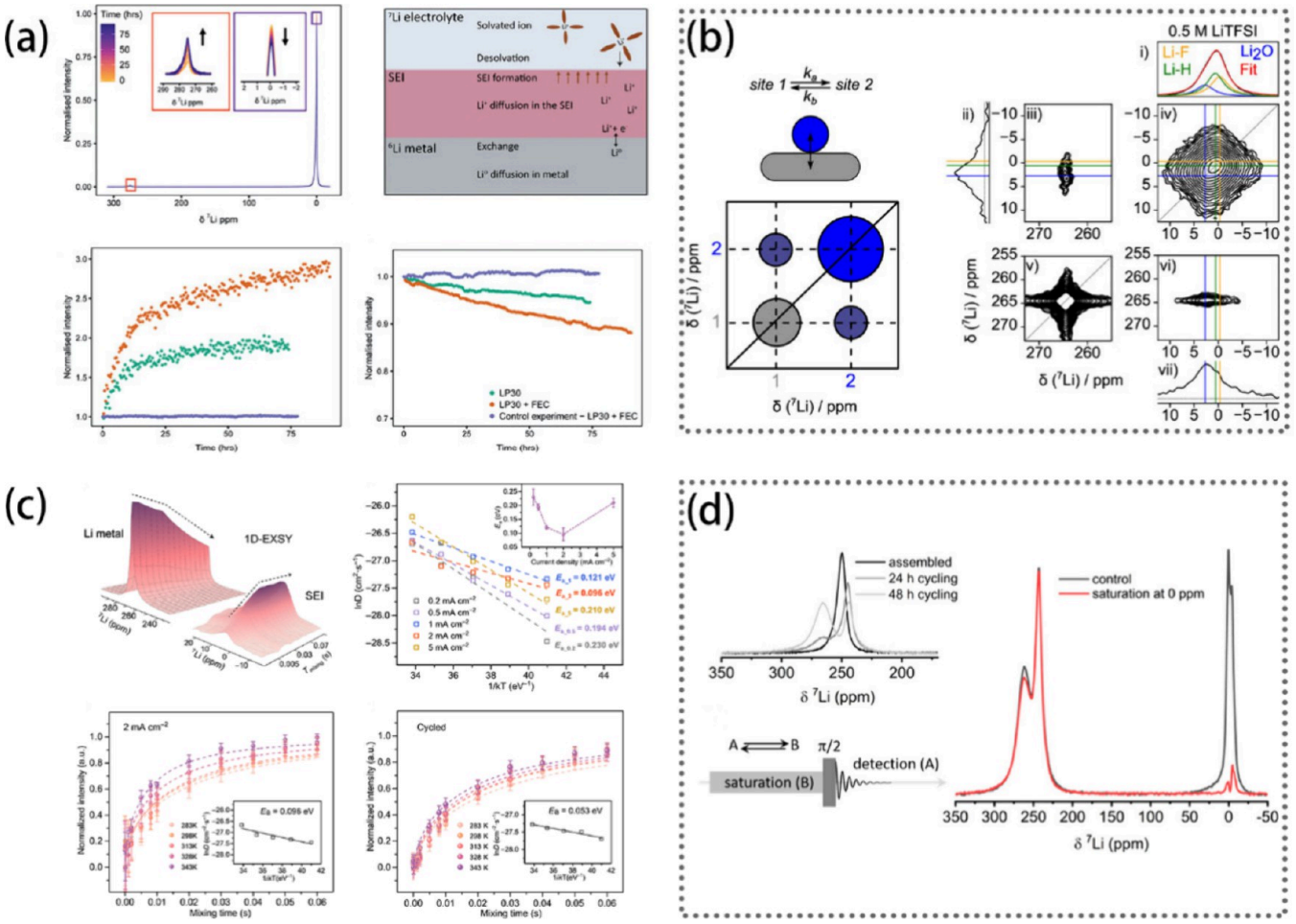

Figure 8. (a) ^{7}Li NMR spectra of the electrolyte (around 0 ppm) and metal (around 275 ppm) and the intensity changes of the lithium metal signal and diamagnetic lithium signal in two electrolytes. Reprinted with permission from ref 71. Copyright 2020 Royal Society of Chemistry. (b) 2D solid-state ^{7}Li−^{7}Li NMR EXSY contour plots showing SEI → metal exchange, SEI ↔ SEI exchange, metal ↔ metal exchange, and metal → SEI exchange, respectively. Reprinted from ref 74. Copyright 2021 American Chemical Society. (c) Quantification of Li-ion diffusion between ED-Li and SEI by ^{7}Li 1D ss NMR exchange experiments. Reprinted with permission from ref 63. Copyright 2024 The American Association for the Advancement of Science. (d) CEST experiments and ^{7}Li NMR spectra of a symmetric battery. Reprinted from ref 76. Copyright 2022 American Chemical Society.

lithium metal interface in the absence of applied voltage.[70] They observed that the NMR spectra showed an increase in the signal of ^{7}Li from the metal and ^{6}Li from the electrolyte, suggesting a spontaneous liquid−solid interfacial ion exchange reaction in this undriven situation (no potential applied). On the basis of this method, Gunnarsdóttir et al. also monitored the exchange between lithium metal and the electrolyte to explore how the different SEI layers formed in two electrolytes affect the rate of isotope exchange[71] (Figure 8a). They developed a numerical model to describe this process, enabling the extraction of exchange current density at the open circuit voltage. The findings revealed that the exchange with the addition of FEC additive is twice as fast as without FEC due to the faster lithium-ion transport within the SEI.

Research has shown that whether the lithium deposition process occurs at a Li−SEI interface or at a fresh Li−electrolyte interface is closely related to the applied current density.[72,73] When lithium metal deposition occurs at the lithium metal/SEI, the composition and structure of the SEI regulate the Li^{+} transport between the lithium metal and electrolyte, with Li^{+} diffusion through the SEI layer being the rate-determining factor. Currently, extensive research is focused on the chemical composition and morphology of the SEI, yet there remains a limited understanding of how the SEI impacts the transfer of Li^{+} at the electrode−electrolyte interface. Traditional methods such as electrochemical impedance spectroscopy have been primarily employed and show limited information and are hard to quantify exactly, while the isotope exchange experiment may introduce disturbances to the formation of the SEI layer, making it challenging to directly measure the local lithium-ion dynamics within the SEI experimentally. Studies have shown that nuclear magnetic resonance exchange spectroscopy can be utilized to determine the exchange rate between the SEI and lithium metal. May et al. reported that spin−lattice (T1) relaxation and exchange spectroscopy (EXSY) NMR measurements revealed that the bisalt electrolyte containing $LiNO_3$ enhances battery electrochemical performance, such as higher Coulombic efficiency, by increasing the Li^{+} exchange rate between lithium metal and SEI (Figure 8b).[74] This effect is attributed to the decomposition product $Li_xN_yO_z$ in the SEI and reduced SEI solubility. Existing research indicates that the initially formed SEI significantly impacts the subsequent cycling performance of lithium metal anodes.[72,75] However, the current under-

https://doi.org/10.1021/acs.jpcc.4c05822
J. Phys. Chem. C 2024, 128, 18659−18677

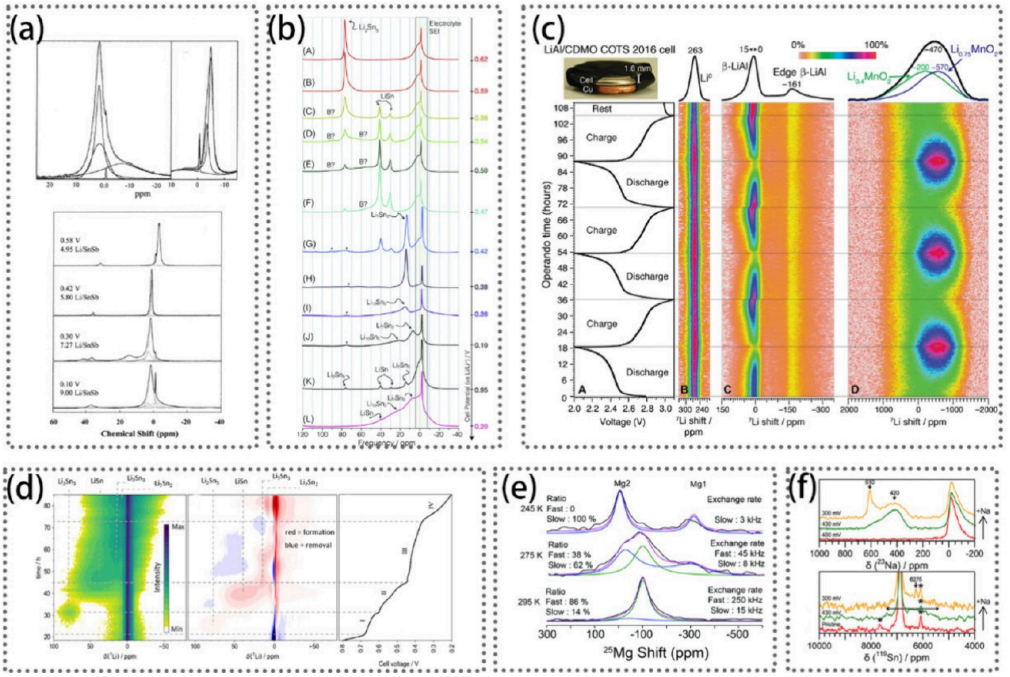

Figure 9. (a) ^{7}Li NMR spectra of Sb and SnSb electrodes discharged to 0 V. Reprinted from ref 78. Copyright 2002 American Chemical Society. (b) *Ex situ* ^{7}Li MAS NMR spectra of different Sn electrodes lithiated to different potentials. Reprinted with permission from ref 85. Copyright 2019 Royal Society of Chemistry. (c) Operando ^{7}Li NMR results for the first three electrochemical cycles of a LiAl/composite dimensional manganese oxide (CDMO) rechargeable commercial off-the-shelf (COTS) coin cell. Reprinted with permission from ref 89. Copyright 2021 The American Association for the Advancement of Science. (d) Operando ^{7}Li NMR measurements and dOp ^{7}Li NMR spectrum of the Sn electrode during the first lithiation. Reprinted from ref 81. Copyright 2021 American Chemical Society. (e) ^{25}Mg VT NMR spectra of the electrochemically prepared Mg_3Bi_2. Reprinted with permission from ref 92. Copyright 2017 Royal Society of Chemistry. (f) *Ex situ* ^{23}Na and ^{119}Sn MAS NMR spectra of tin anodes discharged to 480 mV, 430 mV, and 300 mV. Reprinted from ref 80. Copyright 2017 American Chemical Society.

standing of underlying mechanisms remains incomplete, particularly regarding how the properties of the initially formed SEI affect the Li^+ charge transfer kinetics. Zhang et al. utilized ^{7}Li-^{7}Li 2D exchange ss NMR and variable temperature (VT) exchange ss NMR to quantify Li-ion migration kinetics between electrodeposited Li-metal (ED-Li) and SEI (Figure 8c).[63] The experiments revealed that different formation current densities influence the SEI composition, thereby altering the pathway of lithium-ion transport. Stable cycling performance of the battery can be achieved after activation at moderate current densities (2 mA cm^{-2}), at which point the lithium metal−SEI interface reaches its optimal state. However, the NMR exchange spectroscopy method requires the removal of all or part of the electrolyte from the surface of the SEI, and the SEI in its dry form may exhibit different lithium-ion transport properties compared to the native SEI. In view of this problem, Leskes et al. utilized the chemical exchange saturation transfer (CEST) magnetic resonance imaging (MRI) technique to investigate the lithium-ion exchange process between metallic Li and the native SEI, marking the first application of this method to measure solid−solid interfacial ion exchange (Figure 8d).[76] Compared to 2D exchange spectroscopy, the ^{7}Li-CEST method offers shorter experimental times, enabling direct and efficient comparison of the impact of SEI formed in different electrolytes on the Li permeability. It also allows for the quantitative determination of Li^+ exchange rates between the metal and SEI at different temperatures, further facilitating the calculation of the activation energy required for Li transfer processes.

1.4.4. NMR Application in Other Metal Electrodes Systems. Different from lithium and sodium metals, certain metal or alloy anode materials (such as Sn, Sb, Ge, and Pb) have more mature processing technology and are expected to mitigate the dendrite problem caused by lithium metal or sodium metal deposition due to their high initial voltages.[77] When compared to graphite, alloy anodes have garnered attention due to their high specific capacities. However, during the alloying process, they often form amorphous phases, which pose limitations for many characterization methods. NMR, with its high sensitivity to amorphous phases, holds significant promise for characterizing alloy materials and intermediate products (such as Li-Sn, Li-Sb, Li-Al, and Na-Sn).[78−81]

For lithium-ion battery systems, the evolution of lithium alloying in these metal anodes can be analyzed through ^{7}Li ss NMR. Antimony (Sb) anode, known for its high specific capacity of 660 mAh g^{-1}, abundance of raw materials, ease of preparation, and good safety performance, is considered as promising anode material.[82] Upon discharge to different voltages, the Sb metal anode forms different Li-Sb compounds. ^{7}Li NMR spectra of the Sb reveal two signals at −3.3 and −4.8 ppm when discharged to 0.58 V, corresponding to distinct lithium environments in Li_xSb for x close to 3 (Figure 9a).[78]

Besides, tin (Sn) anodes are also of interest because of their higher specific capacity (993 mAh g^{-1}), longer cycling life, and good resistance to overcharging and overdischarging.[83,84] By operando ^{7}Li NMR and *ex situ* ^{7}Li MAS NMR, Lopez et al. investigated the electrochemical lithiation and delithiation processes of 60 nm Sn particles (Figure 9b).[85] Their study revealed that integrating thermodynamically controlled cyclic voltammetry (CV) experiments with derivative operando (dOp) NMR spectroscopy provided enhanced structural insights compared with conventional operando NMR spectra.

https://doi.org/10.1021/acs.jpcc.4c05822
J. Phys. Chem. C 2024, 128, 18659−18677

During lithiation, they observed a highly disordered phase exhibiting a Knight shift intermediate between Li_2Sn_5 and LiSn, identified as a metastable Li_2Sn_3 phase. Conversely, during delithiation, the operando spectrum displayed narrow resonances for the $Li_{13}Sn_5$ and Li_7Sn_3 phases. Additionally, because of the spin quantum number of Sn atoms being 1/2, the evolution of Sn compounds can also be observed through ^{119}Sn ss NMR spectra. Frerichs et al. employed operando ^{7}Li NMR along with *ex situ* ^{119}Sn MAS NMR measurements to investigate the lithiation mechanism of Sn nanoelectrodes (Figure 9d).[81] The results indicated the presence of the Sn-rich phases Li_2Sn_5 and LiSn at a lithiation potential of 0.50 V, while the Li-rich phase Li_7Sn_3 was observed in both the ^{119}Sn and ^{7}Li NMR spectra at 0.40 V. Upon lithiation to lower voltages, further enhancement in lithiation was observed, and *ex situ* ^{119}Sn and ^{7}Li MAS NMR revealed the formation of disordered Li_xSn phases.

Among the various alloy anode materials, the β-LiAl alloy anode is favored by researchers attributed to several advantages, including a theoretical specific capacity of up to 990 mAh g^{-1}, abundant resource, low-cost, and is environmentally friendly.[86−88] Moreover, the β-LiAl alloy anode exhibits a relatively low volume expansion during cycling, which is conducive to maintaining battery structural stability. Walder et al. conducted operando NMR measurements in coin cells, employing an external NMR coil (Figure 9c).[89] They aimed to observe the real-time lithiation process of β-LiAl electrodes and compare the changes in the β-LiAl ^{7}Li NMR Knight shift and transverse spin relaxation parameter (T_2'). They found that the lithium-ion diffusion rate (positively correlated to T_2' value) decreases with increasing lithium content in β-LiAl, as the increase in lithium content causes fewer lattice vacancies inside β-LiAl. This method is able to relate the lithium-ion dynamics of the material to the compositional changes and also demonstrates the superiority of NMR spectroscopy, which cannot be achieved in other *in situ* methods like *in situ* XRD.

On the other hand, in sodium-ion battery systems, Sn-based anode materials also deliver a specific capacity of 847 mAh g^{-1} (based on $Na_{15}Sn_4$).[90,91] The calculated sodium intercalation potentials of Sn reveal four plateaus corresponding to $NaSn_5$, NaSn, Na_9Sn_4, and $Na_{15}Sn_4$. For a comprehensive understanding of the sodiation mechanism in Sn-based electrodes, Stratford et al. employed ^{23}Na ss NMR and ^{119}Sn ss NMR to investigate the alloying mechanism of Sn-based anode materials in sodium-ion batteries (Figure 9f).[80] Their higher resolution ^{119}Sn MAS NMR spectra exhibited a peak at 6890 ppm, corresponding to residual metallic Sn. As the sodium content increased, a peak emerged at 6275 ppm, indicative of the $NaSn_2$ structure. At the end of discharge, the operando ^{23}Na NMR spectra elucidated the formation of $Na_{15}Sn_4$ observed at −75 ppm, with the potential to store additional sodium atoms as off-stoichiometric compounds ($Na_{15+x}Sn_4$) observed at −260 ppm.

Compared to lithium-ion batteries, magnesium-ion batteries have attracted attention as potential alternatives because of their richer crustal resources and lower cost. However, magnesium metal readily reacts with the electrolyte to form an insulating passivation layer, restricting the transport of electrons and magnesium ions. Therefore, alternative metals are often selected as anode materials for magnesium-ion batteries. Among them, bismuth (Bi) metal anodes have a high theoretical capacity of 385 mAh g^{-1} and a low discharge plateau of 0.2 V versus Mg, allowing them to alloy with Mg to form Mg_3Bi_2. ^{25}Mg ss NMR was utilized to investigate the local structural changes and kinetic information of the Bi electrode during Mg ion alloying processes in magnesium-ion batteries.[92] The results revealed the formation of a Mg_3Bi_2 alloy through the electrochemical process involving Bi nanowires. Furthermore, a rapid exchange between the two Mg sites within the Mg_3Bi_2 structure was observed via ^{25}Mg VT NMR experiments (Figure 9e). On the basis of these observations, a proposed jumping mechanism of Mg1 and Mg2 exchange through the gap tetrahedral sites was suggested.

2. PERSPECTIVE

While solid-state NMR has a unique capability in studying metal anodes, particularly regarding the chemical composition of interphases, deposited morphology, and ion transport across interfaces, several significant limitations listed below hinder its ability to provide a deeper understanding of the failure mechanisms in metal anodes.

2.1. Challenges with *In Situ* NMR Cells. *In situ* NMR studies often require the use of model cells designed to mitigate the skin-depth effects, which can significantly impact the quality of the NMR signal. For example, aluminum-coated bag cells, which have a 10 μm thick aluminum layer, can attenuate the radiofrequency field by up to 70% for lithium resonance at 77 MHz. The problem is even more pronounced with coin cells that use stainless steel casings. While advances in coil and probe design have made it possible to "beat" the skin-depth effect, accurately detecting the inherent electrochemical evolution in commercial multilayer pouch cells remains a significant challenge.

2.2. High Costs and Accessibility of NMR Spectrometers. NMR spectroscopy requires expensive and specialized equipment such as high-field magnets and magic angle spinning (MAS) probes, making it less accessible for routine analysis. In the future, the development of more miniaturized benchtop NMR systems could make *in situ* research on metal anodes more feasible and widespread.

2.3. Correlating SEI Composition with Functionality. Understanding the solid electrolyte interphase (SEI) requires more than just chemical composition analysis: it must be correlated with its function as an ionic conductor. Current methods, such as isotope tracing or chemical exchange saturation transfer (CEST), primarily focus on overall lithium exchange between the metal and SEI. However, the specific ionic transport pathways and rates within individual SEI components, such as LiF, Li_2O, and Li_2CO_3, remain unclear. This gap limits our understanding of how each component contributes to the overall performance and stability of the SEI.

2.4. Sensitivity Limitations. NMR's relatively low sensitivity makes it difficult to detect trace species within the SEI, especially when dealing with nuclei of naturally low abundance, such as ^{13}C, ^{15}N, and ^{6}Li. Improving sensitivity through advanced probe designs and method development (e.g., dynamic nuclear polarization (DNP) or parahydrogen-induced polarization) will be crucial for future research. Enhancing these aspects could enable more detailed studies of the SEI and other crucial interfacial phenomena in lithium metal batteries.

Despite these limitations, NMR remains an invaluable tool in the study of metal anodes, especially when it is used in conjunction with other analytical techniques. For instance,

https://doi.org/10.1021/acs.jpcc.4c05822
J. Phys. Chem. C 2024, 128, 18659−18677

combining NMR with X-ray photoelectron spectroscopy (XPS) can provide detailed interfacial information, while cryo-transmission electron microscopy (cryo-TEM) can offer a high spatial resolution. Additionally, the use of chemical shift calculations could significantly aid in the assignment of different species within overlapping spectra, further enhancing the interpretability of the NMR data.

AUTHOR INFORMATION

Corresponding Authors

Xiangsi Liu − *Research Center for Industries of the Future, Westlake University, Hangzhou 310030 Zhejiang, China; School of Engineering, Westlake University, Hangzhou 310030 Zhejiang, China; Institute of Advanced Technology, Westlake Institute for Advanced Study, Hangzhou 310024 Zhejiang, China*; Email: liuxiangsi@westlake.edu.cn

Yuxuan Xiang − *Research Center for Industries of the Future, Westlake University, Hangzhou 310030 Zhejiang, China; School of Engineering, Westlake University, Hangzhou 310030 Zhejiang, China; Institute of Advanced Technology, Westlake Institute for Advanced Study, Hangzhou 310024 Zhejiang, China*; orcid.org/0000-0001-5741-1546; Email: xiangyuxuan@westlake.edu.cn

Author

Bizhu Zheng − *Research Center for Industries of the Future, Westlake University, Hangzhou 310030 Zhejiang, China; School of Engineering, Westlake University, Hangzhou 310030 Zhejiang, China; Institute of Advanced Technology, Westlake Institute for Advanced Study, Hangzhou 310024 Zhejiang, China*

Complete contact information is available at: https://pubs.acs.org/10.1021/acs.jpcc.4c05822

Notes

The authors declare no competing financial interest.

Biographies

Dr. Bizhu Zheng is currently a postdoctoral researcher at the School of Engineering, Westlake University, Hangzhou. She received her B.S. and Ph.D. degrees from Xiamen University in 2015 and 2020, respectively. Her research interests include the interfacial failure mechanism and modification in lithium/sodium metal batteries.

Dr. Xiangsi Liu received his Ph.D. from Xiamen University in 2022. He then joined Westlake University for postdoctoral research and is currently employed as an Assistant Researcher at the Advanced Characterization Laboratory for Energy Materials of Westlake University. His research interests focus on lithium/sodium-ion layered oxide materials, electrode interface evolution, and applications of solid-state nuclear magnetic resonance techniques.

Dr. Xiang Yuxuan is a Westlake Fellow at the School of Engineering, Westlake University, where he leads the establishment of an advanced characterization laboratory for energy materials. He earned his bachelor's degree in applied chemistry from Nanjing University of Aeronautics and Astronautics in 2016, followed by a Ph.D. from the College of Chemistry and Chemical Engineering at Xiamen University in 2021. His research focuses on the intricate structure-performance relationships of battery materials, utilizing advanced characterization techniques with high spatiotemporal resolution, including *in situ* electrochemical solid-state nuclear magnetic resonance (NMR), high-resolution magic-angle spinning NMR, and mass spectrometry titration techniques. Through these advanced techniques, he aims to provide real-time, quantitative analyses of the failure processes in high-energy-density batteries, contributing to the development of next-generation energy storage solutions.

ACKNOWLEDGMENTS

This work was supported by Research Center for industries of the Future (RCIF) at Westlake University and Westlake Education Foundation, National Natural Science Foundation of China (Grant nos. 22309148 and 22402161).

REFERENCES

(1) Li, S.; Jiang, M.; Xie, Y.; Xu, H.; Jia, J.; Li, J. Developing High-Performance Lithium Metal Anode in Liquid Electrolytes: Challenges and Progress. *Adv. Mater.* **2018**, *30* (17), 1706375.

(2) Wang, H.; Yu, D.; Kuang, C.; Cheng, L.; Li, W.; Feng, X.; Zhang, Z.; Zhang, X.; Zhang, Y. Alkali Metal Anodes for Rechargeable Batteries. *Chem* **2019**, *5* (2), 313−338.

(3) Wu, H.; Jia, H.; Wang, C.; Zhang, J. G.; Xu, W. Recent Progress in Understanding Solid Electrolyte Interphase on Lithium Metal Anodes. *Advanced Energy Materials* **2021**, *11* (5), 2003092.

(4) He, D.; Lu, J.; He, G.; Chen, H. Recent Advances in Solid-Electrolyte Interphase for Li Metal Anode. *Frontiers in Chemistry* **2022**, *10*, 916132.

(5) Li, B.; Chao, Y.; Li, M.; Xiao, Y.; Li, R.; Yang, K.; Cui, X.; Xu, G.; Li, L.; Yang, C.; Yu, Y.; Wilkinson, D. P.; Zhang, J. A Review of Solid Electrolyte Interphase (SEI) and Dendrite Formation in Lithium Batteries. *Electrochemical Energy Reviews* **2023**, *6* (1), 7.

(6) Liu, X.; Liang, Z.; Xiang, Y.; Lin, M.; Li, Q.; Liu, Z.; Zhong, G.; Fu, R.; Yang, Y. Solid-State NMR and MRI Spectroscopy for Li/Na Batteries: Materials, Interface, and In Situ Characterization. *Adv. Mater.* **2021**, *33* (50), 2005878.

(7) Bagheri, K.; Deschamps, M.; Salager, E. Nuclear magnetic resonance for interfaces in rechargeable batteries. *Curr. Opin. Colloid Interface Sci.* **2023**, *64*, 101675.

(8) Pecher, O.; Carretero-González, J.; Griffith, K. J.; Grey, C. P. Materials' Methods: NMR in Battery Research. *Chem. Mater.* **2017**, *29* (1), 213−242.

(9) Haber, S.; Leskes, M. What Can We Learn from Solid State NMR on the Electrode-Electrolyte Interface? *Adv. Mater.* **2018**, *30* (41), 1706496.

(10) Hu, J. Z.; Jaegers, N. R.; Hu, M. Y.; Mueller, K. T. In situ and ex situ NMR for battery research. *Journal of Physics: Condensed Matter* **2018**, *30* (46), 463001.

(11) Levitt, M. H. Spin dynamics: basics of nuclear magnetic resonance. *Wiley*, 2008; pp 1−744.

(12) Wu, N.; Chien, P.-H.; Li, Y.; Dolocan, A.; Xu, H.; Xu, B.; Grundish, N. S.; Jin, H.; Hu, Y.-Y.; Goodenough, J. B. Fast Li+ Conduction Mechanism and Interfacial Chemistry of a NASICON/Polymer Composite Electrolyte. *J. Am. Chem. Soc.* **2020**, *142* (5), 2497−2505.

(13) Kittel, C.; McEuen, P. *Introduction to solid state physics*; *Wiley*, 2004; pp 1−704.

(14) Marchetti, A.; Chen, J.; Pang, Z.; Li, S.; Ling, D.; Deng, F.; Kong, X. Understanding Surface and Interfacial Chemistry in Functional Nanomaterials via Solid-State NMR. *Adv. Mater.* **2017**, *29* (14), 1605895.

(15) Xiang, Y.; Zheng, G.; Liang, Z.; Jin, Y.; Liu, X.; Chen, S.; Zhou, K.; Zhu, J.; Lin, M.; He, H.; et al. Visualizing the growth process of sodium microstructures in sodium batteries by in-situ 23Na MRI and NMR spectroscopy. *Nature Nanotechnology* **2020**, *15* (10), 883−890.

(16) Bhattacharyya, R.; Key, B.; Chen, H.; Best, A. S.; Hollenkamp, A. F.; Grey, C. P. In situ NMR observation of the formation of metallic lithium microstructures in lithium batteries. *Nat. Mater.* **2010**, *9* (6), 504−510.

(17) Hu, J. Z.; Zhao, Z.; Hu, M. Y.; Feng, J.; Deng, X.; Chen, X.; Xu, W.; Liu, J.; Zhang, J.-G. In situ 7Li and 133Cs nuclear magnetic resonance investigations on the role of Cs+ additive in lithium-metal deposition process. *Journal of Power Sources* **2016**, *304*, 51−59.

(18) Bayley, P. M.; Trease, N. M.; Grey, C. P. Insights into Electrochemical Sodium Metal Deposition as Probed with in Situ 23Na NMR. *J. Am. Chem. Soc.* **2016**, *138* (6), 1955−1961.
(19) Haynes, W. *CRC Handbook of Chemistry and Physics*, 95th ed.; CRC Press, 2014; pp 1−2128.
(20) Kubo, A.; Spaniol, T. P.; Terao, T. The Effect of Bulk Magnetic Susceptibility on Solid State NMR Spectra of Paramagnetic Compounds. *J. Magn. Reson.* **1998**, *133*, 330−340.
(21) Zhou, L.; Leskes, M.; Ilott, A. J.; Trease, N. M.; Grey, C. P. Paramagnetic electrodes and bulk magnetic susceptibility effects in the in situ NMR studies of batteries: Application to Li1.08Mn1.92O4 spinels. *J. Magn. Reson.* **2013**, *234*, 44−57.
(22) Trease, N. M.; Zhou, L.; Chang, H. J.; Zhu, B. Y.; Grey, C. P. In situ NMR of lithium ion batteries: Bulk susceptibility effects and practical considerations. *Solid State Nucl. Magn. Reson.* **2012**, *42*, 62−70.
(23) Tao, M.; Chen, X.; Lin, H.; Jin, Y.; Shan, P.; Zhao, D.; Gao, M.; Liang, Z.; Yang, Y. Clarifying the Temperature-Dependent Lithium Deposition/Stripping Process and the Evolution of Inactive Li in Lithium Metal Batteries. *ACS Nano* **2023**, *17* (23), 24104−24114.
(24) Liang, Z.; Xiang, Y.; Wang, K.; Zhu, J.; Jin, Y.; Wang, H.; Zheng, B.; Chen, Z.; Tao, M.; Liu, X.; Wu, Y.; Fu, R.; Wang, C.; Winter, M.; Yang, Y. Understanding the failure process of sulfide-based all-solid-state lithium batteries via operando nuclear magnetic resonance spectroscopy. *Nature Communications* **2023**, *14*, 259.
(25) Chang, H. J.; Trease, N. M.; Ilott, A. J.; Zeng, D.; Du, L.-S.; Jerschow, A.; Grey, C. P. Investigating Li Microstructure Formation on Li Anodes for Lithium Batteries by in Situ 6Li/7Li NMR and SEM. *The Journal of Physical Chemistry C* **2015**, *119* (29), 16443−16451.
(26) Chiou, M.-H.; Verweyen, E.; Diddens, D.; Wichmann, L.; Schmidt, C.; Neuhaus, K.; Choudhary, A.; Bedrov, D.; Winter, M.; Brunklaus, G. Selection of Polymer Segment Species Matters for Electrolyte Properties and Performance in Lithium Metal Batteries. *ACS Applied Energy Materials* **2023**, *6* (8), 4422−4436.
(27) KüPers, V.; Kolek, M.; Bieker, P.; Winter, M.; Brunklaus, G. In situ7Li-NMR analysis of lithium metal surface deposits with varying electrolyte compositions and concentrations. *Phys. Chem. Chem. Phys.* **2019**, *21* (47), 26084−26094.
(28) Lennartz, P.; Borzutzki, K.; Winter, M.; Brunklaus, G. Viscoelastic polyborosiloxanes as artificial solid electrolyte interphase on lithium metal anodes. *Electrochim. Acta* **2021**, *388*, 138526.
(29) Wang, C.; Liu, M.; Thijs, M.; Ooms, F. G. B.; Ganapathy, S.; Wagemaker, M. High dielectric barium titanate porous scaffold for efficient Li metal cycling in anode-free cells. *Nature Communications* **2021**, *12*, 6536.
(30) Wang, Q.; Zhao, C.; Wang, S.; Wang, J.; Liu, M.; Ganapathy, S.; Bai, X.; Li, B.; Wagemaker, M. Clarifying the Relationship between the Lithium Deposition Coverage and Microstructure in Lithium Metal Batteries. *J. Am. Chem. Soc.* **2022**, *144* (48), 21961−21971.
(31) Lin, X.; Shen, Y.; Yu, Y.; Huang, Y. In Situ NMR Verification for Stacking Pressure-Induced Lithium Deposition and Dead Lithium in Anode-Free Lithium Metal Batteries. *Advanced Energy Materials* **2024**, *14* (14), 2303918.
(32) Chandrashekar, S.; Trease, N. M.; Chang, H. J.; Du, L.-S.; Grey, C. P.; Jerschow, A. 7Li MRI of Li batteries reveals location of microstructural lithium. *Nature materials* **2012**, *11* (4), 311−315.
(33) Chang, H. J.; Ilott, A. J.; Trease, N. M.; Mohammadi, M.; Jerschow, A.; Grey, C. P. Correlating Microstructural Lithium Metal Growth with Electrolyte Salt Depletion in Lithium Batteries Using 7Li MRI. *J. Am. Chem. Soc.* **2015**, *137* (48), 15209−15216.
(34) Marbella, L. E.; Zekoll, S.; Kasemchainan, J.; Emge, S. P.; Bruce, P. G.; Grey, C. P. 7Li NMR Chemical Shift Imaging To Detect Microstructural Growth of Lithium in All-Solid-State Batteries. *Chem. Mater.* **2019**, *31* (8), 2762−2769.
(35) Ilott, A. J.; Mohammadi, M.; Chang, H. J.; Grey, C. P.; Jerschow, A. Real-time 3D imaging of microstructure growth in battery cells using indirect MRI. *Proceedings of the National Academy of Sciences* **2016**, *113* (39), 10779−10784.
(36) Pecher, O.; Bayley, P. M.; Liu, H.; Liu, Z.; Trease, N. M.; Grey, C. P. Automatic Tuning Matching Cycler (ATMC) in situ NMR spectroscopy as a novel approach for real-time investigations of Li- and Na-ion batteries. *J. Magn. Reson.* **2016**, *265*, 200−209.
(37) Bray, J. M.; Doswell, C. L.; Pavlovskaya, G. E.; Chen, L.; Kishore, B.; Au, H.; Alptekin, H.; Kendrick, E.; Titirici, M.-M.; Meersmann, T.; Britton, M. M.; et al. Operando visualisation of battery chemistry in a sodium-ion battery by 23Na magnetic resonance imaging. *Nature Communications* **2020**, *11* (1), 2083.
(38) Rees, G. J.; Spencer Jolly, D.; Ning, Z.; Marrow, T. J.; Pavlovskaya, G. E.; Bruce, P. G. Imaging Sodium Dendrite Growth in All-Solid-State Sodium Batteries Using 23Na T2-Weighted Magnetic Resonance Imaging. *Angewandte Chemie International Edition* **2021**, *60* (4), 2110−2115.
(39) Hsieh, Y.-C.; Leißing, M.; Nowak, S.; Hwang, B.-J.; Winter, M.; Brunklaus, G. Quantification of Dead Lithium via In Situ Nuclear Magnetic Resonance Spectroscopy. *Cell Reports Physical Science* **2020**, *1* (8), 100139.
(40) Gunnarsdóttir, A. B.; Amanchukwu, C. V.; Menkin, S.; Grey, C. P. Noninvasive In Situ NMR Study of "Dead Lithium" Formation and Lithium Corrosion in Full-Cell Lithium Metal Batteries. *J. Am. Chem. Soc.* **2020**, *142* (49), 20814−20827.
(41) Fang, C.; Li, J.; Zhang, M.; Zhang, Y.; Yang, F.; Lee, J. Z.; Lee, M.-H.; Alvarado, J.; Schroeder, M. A.; Yang, Y.; et al. Quantifying inactive lithium in lithium metal batteries. *Nature* **2019**, *572* (7770), 511−515.
(42) Xiang, Y.; Tao, M.; Zhong, G.; Liang, Z.; Zheng, G.; Huang, X.; Liu, X.; Jin, Y.; Xu, N.; Armand, M.; Zhang, J.-G.; Xu, K.; Fu, R.; Yang, Y.; et al. Quantitatively analyzing the failure processes of rechargeable Li metal batteries. *Science Advances* **2021**, *7* (46), No. eabj3423.
(43) Wang, Q.; Zhao, C.; Wang, J.; Yao, Z.; Wang, S.; Kumar, S. G. H.; Ganapathy, S.; Eustace, S.; Bai, X.; Li, B.; Wagemaker, M.; et al. High entropy liquid electrolytes for lithium batteries. *Nature Communications* **2023**, *14*, 440.
(44) Arai, J.; Okada, Y.; Sugiyama, T.; Izuka, M.; Gotoh, K.; Takeda, K. In Situ Solid State 7Li NMR Observation of Lithium Metal Deposition during Overcharge in Lithium Ion Battery. *J. Electrochem. Soc.* **2015**, *162* (6), A952−A958.
(45) Gotoh, K.; Izuka, M.; Arai, J.; Okada, Y.; Sugiyama, T.; Takeda, K.; Ishida, H. In situ 7Li nuclear magnetic resonance study of the relaxation effect in practical lithium ion batteries. *Carbon* **2014**, *79*, 380−387.
(46) Sanders, K. J.; Ciezki, A. A.; Berno, A.; Halalay, I. C.; Goward, G. R. Quantitative Operando 7Li NMR Investigations of Silicon Anode Evolution during Fast Charging and Extended Cycling. *J. Am. Chem. Soc.* **2023**, *145* (39), 21502−21513.
(47) Mei, W.; Jiang, L.; Liang, C.; Sun, J.; Wang, Q. Understanding of Li-plating on graphite electrode: detection, quantification and mechanism revelation. *Energy Storage Materials* **2021**, *41*, 209−221.
(48) Fang, Y.; Smith, A. J.; Lindström, R. W.; Lindbergh, G.; Furó, I. Quantifying lithium lost to plating and formation of the solid-electrolyte interphase in graphite and commercial battery components. *Applied Materials Today* **2022**, *28*, 101527.
(49) Arai, J.; Nakahigashi, R. Study of Li Metal Deposition in Lithium Ion Battery during Low-Temperature Cycle Using In Situ Solid-State7Li Nuclear Magnetic Resonance. *Journal of The Electrochemical Society* **2017**, *164* (13), A3403−A3409.
(50) Krachkovskiy, S. A.; Reza, M.; Aguilera, A. R.; Halalay, I. C.; Balcom, B. J.; Goward, G. R. Real-Time Quantitative Detection of Lithium Plating by In Situ NMR Using a Parallel-Plate Resonator. *Journal of The Electrochemical Society* **2020**, *167* (13), 130514.
(51) Gotoh, K.; Yamakami, T.; Nishimura, I.; Kometani, H.; Ando, H.; Hashi, K.; Shimizu, T.; Ishida, H. Mechanisms for overcharging of carbon electrodes in lithium-ion/sodium-ion batteries analysed by operando solid-state NMR. *Journal of Materials Chemistry A* **2020**, *8* (29), 14472−14481.
(52) Freytag, A. I.; Pauric, A. D.; Krachkovskiy, S. A.; Goward, G. R. In Situ Magic-Angle Spinning 7Li NMR Analysis of a Full

Electrochemical Lithium-Ion Battery Using a Jelly Roll Cell Design. *J. Am. Chem. Soc.* **2019**, *141* (35), 13758−13761.
(53) Märker, K.; Xu, C.; Grey, C. P. Operando NMR of NMC811/Graphite Lithium-Ion Batteries: Structure, Dynamics, and Lithium Metal Deposition. *J. Am. Chem. Soc.* **2020**, *142* (41), 17447−17456.
(54) Zhang, Z.; Tian, J.; Chen, J.; He, Y.; Liu, C.; Liang, X.; Feng, J. Li Plating on Carbon Electrode Surface Probed by Low-Field Dynamic Nuclear Polarization 7Li NMR. *Chin. Phys. Lett.* **2021**, *38* (12), 126801.
(55) Stratford, J. M.; Allan, P. K.; Pecher, O.; Chater, P. A.; Grey, C. P. Mechanistic insights into sodium storage in hard carbon anodes using local structure probes. *Chemical Communications* **2016**, *52* (84), 12430−12433.
(56) Morita, R.; Gotoh, K.; Kubota, K.; Komaba, S.; Hashi, K.; Shimizu, T.; Ishida, H. Correlation of carbonization condition with metallic property of sodium clusters formed in hard carbon studied using 23Na nuclear magnetic resonance. *Carbon* **2019**, *145*, 712−715.
(57) Kamiyama, A.; Kubota, K.; Igarashi, D.; Youn, Y.; Tateyama, Y.; Ando, H.; Gotoh, K.; Komaba, S. MgO-Template Synthesis of Extremely High Capacity Hard Carbon for Na-Ion Battery. *Angewandte Chemie International Edition* **2021**, *60* (10), 5114−5120.
(58) Li, Q.; Liu, X.; Tao, Y.; Huang, J.; Zhang, J.; Yang, C.; Zhang, Y.; Zhang, S.; Jia, Y.; Lin, Q.; Xiang, Y.; Cheng, J.; Lv, W.; Kang, F.; Yang, Y.; Yang, Q.-H. Sieving carbons promise practical anodes with extensible low-potential plateaus for sodium batteries. *National Science Review* **2022**, *9* (8), nwac084.
(59) Qian, J.; Adams, B. D.; Zheng, J.; Xu, W.; Henderson, W. A.; Wang, J.; Bowden, M. E.; Xu, S.; Hu, J.; Zhang, J. G. Anode-Free Rechargeable Lithium Metal Batteries. *Advanced Functional Materials* **2016**, *26* (39), 7094−7102.
(60) Wan, C.; Xu, S.; Hu, M. Y.; Cao, R.; Qian, J.; Qin, Z.; Liu, J.; Mueller, K. T.; Zhang, J.-G.; Hu, J. Z. Multinuclear NMR Study of the Solid Electrolyte Interface Formed in Lithium Metal Batteries. *ACS Applied Materials & Interfaces* **2017**, *9* (17), 14741−14748.
(61) Zheng, B.; Liu, X.; Zhu, J.; Zhao, J.; Zhong, G.; Xiang, Y.; Wang, H.; Zhao, W.; Umeshbabu, E.; Wu, Q.-H.; et al. Unraveling (electro)-chemical stability and interfacial reactions of Li10SnP2S12 in all-solid-state Li batteries. *Nano Energy* **2020**, *67*, 104252.
(62) Hope, M. A.; Rinkel, B. L. D.; Gunnarsdóttir, A. B.; Märker, K.; Menkin, S.; Paul, S.; Sergeyev, I. V.; Grey, C. P. Selective NMR observation of the SEI-metal interface by dynamic nuclear polarisation from lithium metal. *Nature Communications* **2020**, *11* (1), 2224.
(63) Zhang, S.; Li, Y.; Bannenberg, L. J.; Liu, M.; Ganapathy, S.; Wagemaker, M. The lasting impact of formation cycling on the Li-ion kinetics between SEI and the Li-metal anode and its correlation with efficiency. *Science Advances* **2024**, *10* (3), No. eadj8889.
(64) May, R.; Zhang, Y.; Denny, S. R.; Viswanathan, V.; Marbella, L. E. Leveraging Cation Identity to Engineer Solid Electrolyte Interphases for Rechargeable Lithium Metal Anodes. *Cell Reports Physical Science* **2020**, *1* (11), 100239.
(65) Girard, G. M. A.; Hilder, M.; Dupre, N.; Guyomard, D.; Nucciarone, D.; Whitbread, K.; Zavorine, S.; Moser, M.; Forsyth, M.; MacFarlane, D. R.; et al. Spectroscopic Characterization of the SEI Layer Formed on Lithium Metal Electrodes in Phosphonium Bis(fluorosulfonyl)imide Ionic Liquid Electrolytes. *ACS Applied Materials & Interfaces* **2018**, *10* (7), 6719−6729.
(66) Cao, R.; Mishra, K.; Li, X.; Qian, J.; Engelhard, M. H.; Bowden, M. E.; Han, K. S.; Mueller, K. T.; Henderson, W. A.; Zhang, J.-G. Enabling room temperature sodium metal batteries. *Nano Energy* **2016**, *30*, 825−830.
(67) Gao, L.; Chen, J.; Liu, Y.; Yamauchi, Y.; Huang, Z.; Kong, X. Revealing the chemistry of an anode-passivating electrolyte salt for high rate and stable sodium metal batteries. *Journal of Materials Chemistry A* **2018**, *6* (25), 12012−12017.
(68) Ferdousi, S. A.; O'Dell, L. A.; Hilder, M.; Barlow, A. J.; Armand, M.; Forsyth, M.; Howlett, P. C. SEI Formation on Sodium Metal Electrodes in Superconcentrated Ionic Liquid Electrolytes and the Effect of Additive Water. *ACS Applied Materials & Interfaces* **2021**, *13* (4), 5706−5720.
(69) Gao, L.; Chen, J.; Chen, Q.; Kong, X. The chemical evolution of solid electrolyte interface in sodium metal batteries. *Science Advances* **2022**, *8* (6), No. eabm4606.
(70) Ilott, A. J.; Jerschow, A. Probing Solid-Electrolyte Interphase (SEI) Growth and Ion Permeability at Undriven Electrolyte-Metal Interfaces Using 7Li NMR. *The Journal of Physical Chemistry C* **2018**, *122* (24), 12598−12604.
(71) Gunnarsdóttir, A. B.; Vema, S.; Menkin, S.; Marbella, L. E.; Grey, C. P. Investigating the effect of a fluoroethylene carbonate additive on lithium deposition and the solid electrolyte interphase in lithium metal batteries using in situ NMR spectroscopy. *Journal of Materials Chemistry A* **2020**, *8* (30), 14975−14992.
(72) Boyle, D. T.; Li, Y.; Pei, A.; Vilá, R. A.; Zhang, Z.; Sayavong, P.; Kim, M. S.; Huang, W.; Wang, H.; Liu, Y.; et al. Resolving Current-Dependent Regimes of Electroplating Mechanisms for Fast Charging Lithium Metal Anodes. *Nano Letters* **2022**, *22* (20), 8224−8232.
(73) Shi, F.; Pei, A.; Boyle, D. T.; Xie, J.; Yu, X.; Zhang, X.; Cui, Y. Lithium metal stripping beneath the solid electrolyte interphase. *Proceedings of the National Academy of Sciences* **2018**, *115* (34), 8529−8534.
(74) May, R.; Fritzsching, K. J.; Livitz, D.; Denny, S. R.; Marbella, L. E. Rapid Interfacial Exchange of Li Ions Dictates High Coulombic Efficiency in Li Metal Anodes. *ACS Energy Letters* **2021**, *6* (4), 1162−1169.
(75) Hobold, G. M.; Kim, K.-H.; Gallant, B. M. Beneficial vs. inhibiting passivation by the native lithium solid electrolyte interphase revealed by electrochemical Li+ exchange. *Energy & Environmental Science* **2023**, *16* (5), 2247−2261.
(76) Columbus, D.; Arunachalam, V.; Glang, F.; Avram, L.; Haber, S.; Zohar, A.; Zaiss, M.; Leskes, M. Direct Detection of Lithium Exchange across the Solid Electrolyte Interphase by 7Li Chemical Exchange Saturation Transfer. *J. Am. Chem. Soc.* **2022**, *144* (22), 9836−9844.
(77) Li, W.; Sun, X.; Yu, Y. Si-, Ge-, Sn-Based Anode Materials for Lithium-Ion Batteries: From Structure Design to Electrochemical Performance. *Small Methods* **2017**, *1* (3), 1600037.
(78) Fernández-Madrigal, F. J.; Lavela, P.; Vicente, C. P.; Tirado, J. L.; Jumas, J. C.; Olivier-Fourcade, J. X-ray Diffraction, 7Li MAS NMR Spectroscopy, and 119Sn Mössbauer Spectroscopy Study of SnSb-Based Electrode Materials. *Chem. Mater.* **2002**, *14* (7), 2962−2968.
(79) Chumak, I.; Dmytriv, G.; Pavlyuk, V.; Oswald, S.; Eckert, J.; Trill, H.; Eckert, H.; Pauly, H.; Ehrenberg, H. Li(Al1-zZnz) alloys as anode materials for rechargeable Li-ion batteries. *J. Mater. Res.* **2010**, *25* (8), 1492−1499.
(80) Stratford, J. M.; Mayo, M.; Allan, P. K.; Pecher, O.; Borkiewicz, O. J.; Wiaderek, K. M.; Chapman, K. W.; Pickard, C. J.; Morris, A. J.; Grey, C. P. Investigating Sodium Storage Mechanisms in Tin Anodes: A Combined Pair Distribution Function Analysis, Density Functional Theory, and Solid-State NMR Approach. *J. Am. Chem. Soc.* **2017**, *139* (21), 7273−7286.
(81) Frerichs, J. E.; Ruttert, M.; Böckmann, S.; Winter, M.; Placke, T.; Hansen, M. R. Identification of LixSn Phase Transitions During Lithiation of Tin Nanoparticle-Based Negative Electrodes from Ex Situ 119Sn MAS NMR and Operando 7Li NMR and XRD. *ACS Applied Energy Materials* **2021**, *4* (7), 7278−7287.
(82) He, M.; Kravchyk, K.; Walter, M.; Kovalenko, M. V. Monodisperse Antimony Nanocrystals for High-Rate Li-ion and Na-ion Battery Anodes: Nano versus Bulk. *Nano Letters* **2014**, *14* (3), 1255−1262.
(83) Wang, B.; Luo, B.; Li, X.; Zhi, L. The dimensionality of Sn anodes in Li-ion batteries. *Materials Today* **2012**, *15* (12), 544−552.
(84) Hu, R.; Liu, H.; Zeng, M.; Liu, J.; Zhu, M. Progress on Sn-based thin-film anode materials for lithium-ion batteries. *Chin. Sci. Bull.* **2012**, *57* (32), 4119−4130.
(85) Lorie Lopez, J. L.; Grandinetti, P. J.; Co, A. C. Phase transformations and capacity fade mechanism in LixSn nanoparticle electrodes revealed by operando7Li NMR. *Journal of Materials Chemistry A* **2019**, *7* (17), 10781−10794.

https://doi.org/10.1021/acs.jpcc.4c05822
J. Phys. Chem. C 2024, 128, 18659−18677

(86) Zheng, T.; Boles, S. T. Lithium aluminum alloy anodes in Li-ion rechargeable batteries: Past developments, recent progress, and future prospects. *Progress in Energy* **2023**, *5* (3), 032001.
(87) Wells, L.; Pham, T. A.; Eshetu, G. G.; Seidlmayer, S.; Ceccio, G.; Cannavo, A.; Vacik, J.; Mikitisin, A.; Muller-Buschbaum, P.; Gilles, R.; Figgemeier, E.; et al. Unraveling the Role and Impact of Alumina on the Nucleation and Reversibility of β-LiAl in Aluminum Anode Based Lithium-Ion Batteries. *ChemElectroChem* **2024**, *11*, No. e202400322.
(88) Zheng, T.; Kramer, D.; Mönig, R.; Boles, S. T. Aluminum Foil Anodes for Li-Ion Rechargeable Batteries: the Role of Li Solubility within β-LiAl. *ACS Sustainable Chemistry & Engineering* **2022**, *10* (10), 3203−3210.
(89) Walder, B. J.; Conradi, M. S.; Borchardt, J. J.; Merrill, L. C.; Sorte, E. G.; Deichmann, E. J.; Anderson, T. M.; Alam, T. M.; Harrison, K. L. NMR spectroscopy of coin cell batteries with metal casings. *Science Advances* **2021**, *7* (37), No. eabg8298.
(90) Nam, D.-H.; Hong, K.-S.; Lim, S.-J.; Kim, T.-H.; Kwon, H.-S. Electrochemical Properties of Electrodeposited Sn Anodes for Na-Ion Batteries. *The Journal of Physical Chemistry C* **2014**, *118* (35), 20086−20093.
(91) Ying, H.; Han, W. Q. Metallic Sn-Based Anode Materials: Application in High-Performance Lithium-Ion and Sodium-Ion Batteries. *Advanced Science* **2017**, *4* (11), 1700298.
(92) Liu, Z.; Lee, J.; Xiang, G.; Glass, H. F. J.; Keyzer, E. N.; Dutton, S. E.; Grey, C. P. Insights into the electrochemical performances of Bi anodes for Mg ion batteries using 25Mg solid state NMR spectroscopy. *Chemical Communications* **2017**, *53* (4), 743−746.

https://doi.org/10.1021/acs.jpcc.4c05822
J. Phys. Chem. C 2024, 128, 18659−18677